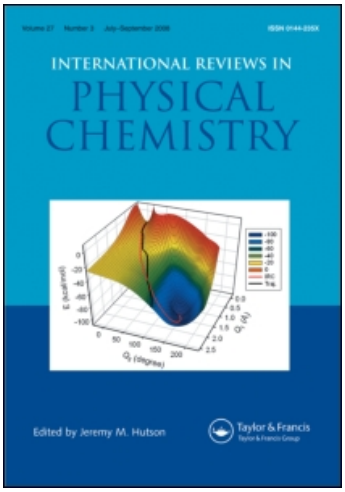

International Reviews in Physical Chemistry
Publication details, including instructions for authors and subscription information:
http://www.informaworld.com/smpp/title~content=t713724383

Random and ordered arrays of surface magic clusters

Y. L. Wang[a]; A. A. Saranin[b]; A. V. Zotov[b]; M. Y. Lai[a]; H. H. Chang[a]
[a] Institute of Atomic and Molecular Sciences, Academia Sinica, Taipei 10617, Taiwan [b] Institute of Automation and Control Processes Far Eastern Branch of Russian Academy of Sciences, Vladivostok 690041, Russian Federation

To cite this Article Wang, Y. L. , Saranin, A. A. , Zotov, A. V. , Lai, M. Y. and Chang, H. H.(2008) 'Random and ordered arrays of surface magic clusters', International Reviews in Physical Chemistry, 27: 2, 317 — 360
To link to this Article: DOI: 10.1080/01442350801943708
URL: http://dx.doi.org/10.1080/01442350801943708

International Reviews in Physical Chemistry
Vol. 27, No. 2, April–June 2008, 317–360

Taylor & Francis
Taylor & Francis Group

Random and ordered arrays of surface magic clusters

Y. L. Wang[a]*, A. A. Saranin[b], A. V. Zotov[b], M. Y. Lai[a] and H. H. Chang[a]

[a]*Institute of Atomic and Molecular Sciences, Academia Sinica, Taipei 10617, Taiwan;*
[b]*Institute of Automation and Control Processes Far Eastern Branch of Russian Academy of Sciences, Vladivostok 690041, Russian Federation*

(*Received 15 December 2007; final version received 25 January 2008*)

Surface magic clusters (SMCs) are clusters exhibiting enhanced stability at certain sizes on a particular surface. Through the formation of SMCs, it is possible to grow an ensemble of nanostructures on a surface with extremely small or essentially zero size dispersion. Such an ensemble of nanostructures with identical size and atomic structure is highly desirable for certain nanotechnologies that rely on the homogeneity in the physical and chemical properties of the constituent nanostructures. This review summarizes current experimental observations and understanding of SMCs and discusses the most recent progress in the formation of a two-dimensional lattice of SMCs, whose constituent clusters have not only identical size and structure but also the same local environment due to the translational symmetry of the system.

Keywords: nanoclustering; self-assembly; self-organization; silicon; single crystal surfaces; surface magic clusters

Contents

*Corresponding author. Email: ylwang@pub.iams.sinica.edu.tw

ISSN 0144–235X print/ISSN 1366–591X online

DOI: 10.1080/01442350801943708
http://www.informaworld.com

1. Introduction

One of the most critical challenges in nanoscience and nanotechnology is to be able to fabricate an ensemble of nanostructures with identical size and atomic structure because the physical and chemical properties of a nanostructure are expected to change significantly with slight variation in its size or structure. From the view point of nanofabrication, this ability to control the number and configuration of the constituent atoms in the desired nanostructures as well as their environment should be considered as the ultimate goal of nanofabrication. Although techniques for nanofabrication based on photon, electron, or ion beams have been employed for the fabrication of structures with ~10 nm lateral resolution, intrinsic limitations of these so-called 'top-down' fabrication techniques appear insurmountable in the near future [1]. The employment of scanning probe microscopes (SPM) as lithographic tools have shown exciting possibilities of single atom manipulation [2,3] and atomic scale chemistry [4–6]. However, the intrinsically slow speed of such serial writing methods presents very serious challenges. The alternative 'bottom-up' approach by assembly of nanostructures from its constituent atoms and/or molecules is conceptually attractive since it is intrinsically a parallel process [7–10] and, in principle, a large quantity of the desired nanostructures can be fabricated simultaneously. However, the size and atomic structure of the assembled nanostructures still suffer from large variation in most cases and the spatial arrangements of the nanostructures are even harder to control. Typically, the size dispersion ΔS (full width at half maximum in the size distribution curve) of nanostructures fabricated by different methods, such as vapour deposition of materials onto surfaces, is usually larger than one half of the average size (S_a). Here, for clarity and consistency, we choose to define the size of a nanostructure as its total number of atoms rather than its characteristic linear dimension adapted by many authors. Significant reduction in the ΔS of an ensemble of nanostructures has been demonstrated in certain material systems by exploiting the strain on the substrate surface or in the nanostructures [11–13]. Nevertheless, the $\Delta S/S_a$ is still larger than what is desired for most fundamental studies in nanoscience and potential applications in nanotechnology. Ensembles of nanostructures with ΔS ~10% and good ordering in the spatial arrangement are achieved only in a few cases [14]. Therefore, methods for controlling the size and structure uniformity of an ensemble of nanostructures, and the precision in their spatial arrangement are highly desirable for further advancement of nanoscience and nanotechnology.

Magic clusters, i.e., clusters with enhanced stability at certain sizes, were discovered by mass spectrometry more than two decades ago [15,16]. Numerous researches have been devoted to the subject; and it has been known for some time that the enhanced stability

at certain sizes originates from either the electronic or atomic shell closure of a cluster with magic number of constituent atoms. Intuitively, such clusters with enhanced stability could be exploited for the growth of nanostructures on surfaces with very narrow size dispersion. However, the shell closure and corresponding enhanced stability of a magic cluster could be destroyed by the cluster-surface interaction when it is brought into contact with a certain surface. For example, Na_8 is a magic cluster in free space, its enhanced stability is predicted to be destroyed when landed on a Na(100) surface but maintained on a NaCl(100) surface [17]. Therefore, the role of the substrate surface must be carefully considered when attempting to place or grow magic clusters on a particular surface.

Surface magic clusters (SMCs), i.e., clusters with enhanced stability at certain sizes on a particular surface, have caught the attention of the scientific community [18] since their first discovery of SMCs on the $\sqrt{3} \times \sqrt{3}R30^\circ$-reconstructed Ga/Si(111) surface in 1998. The subject has been reviewed recently with an emphasis on exploiting the formation of SMCs as a pathway to grow mono-dispersed nanostructures on a particular surface [19]. To avoid unnecessary duplication, this review will only briefly summarize the highlights of the previous efforts that are needed for a self-contained introduction to the recent developments in the field of SMCs and related subjects. In particular, it attempts to point out the equal partnership between the adsorbates and substrate surface in constraining the self-organized growth of SMCs, especially the interplay between the partners in the formation of two-dimensional (2D) lattices of SMCs. Although we have attempted to include most of the relevant literatures in this review, it is not meant to be an exhaustive recollection. Its contents primarily reflect the viewpoints of experimentalists about the subject of random and ordered arrays of SMCs, and to some extent, the implications of such a uniform array of nanostructures to the development of nanoscience and nanotechnology.

We would like to remark that the present review emphasizes the magic clustering on silicon (i.e., semiconductor) surfaces. Most of the SMCs formed on Si appeared to display semiconducting properties. This suggests that the SMC formation is controlled mainly by atomic bonding via localized valence electrons and the collective electron effects are not expected to play essential roles. Therefore, the reduction of the dangling bond number is believed to play the most important role in minimizing the system energy. In contrast, the situation might be opposite for the metal clusters formed on metal surfaces, where SMC formation could be controlled mainly by electronic shell closing. More sophisticated situations are also possible as, for example, in the case of the Ag-SMC growth on the metallic Pb/Si(111) surface [20], where the origin of the magic numbers of the 2D metal clusters evolves from electronic to geometric shell closure with increasing SMC size.

2. Randomly distributed Ga-induced SMCs on Ga/Si(111) $\sqrt{3} \times \sqrt{3}$

Speculation about the existence of SMC was raised more than a decade ago in a report on the abnormal signal of He scattered from the Pt/Pt(111) surface [21]. However, no sign of SMC was observed in the later scanning tunnelling microscopy (STM) studies of this system [22]. The existence of SMC was unambiguously demonstrated in an experiment in which Ga was deposited onto the $\sqrt{3} \times \sqrt{3}R30^\circ$-reconstructed Ga/Si(111) surface to induce the formation of clusters with enhanced stability [23,24]. This experiment was

followed by the observation of Si-islands with magic number of 7×7 unit cells on the Si(111) surface [25]; and the careful examination of a type of Si-clusters on the Si(111) surface [26]. One of the common features of the SMCs reported in these pioneering experiments on SMC was that the clusters were randomly distributed on the surface. In the following, highlights of such randomly distributed SMCs are reviewed with an emphasis on the role of the atoms in the environment of the SMCs. Specifically, how the chemical bonding on these atoms affects the structural stability of a SMC and its neighbouring area, which has important implications for the growth of an ordered array of identical SMC on a particular substrate surface.

Various surface reconstructions induced by the deposition of Ga onto a Si(111)7×7 surface have been studied extensively since the 1980s [27–35]. These early studies provided two important pieces of information that paved the way for the first discovery of SMC. (In retrospect, the fact that SMC in this material system remained unnoticed until 1998 is partly due to the recent paradigm shift towards nanoscience in the field of surface science.) First, deposition of a ~1/3 monolayer (ML) ($1\,\mathrm{ML} = 7.83 \times 10^{14}\,\mathrm{cm}^{-2}$) of Ga and subsequent annealing at ~550°C leads to the formation of Si(111)$\sqrt{3} \times \sqrt{3}R30°$-Ga surface reconstruction which is well-established to be built of Ga adatoms occupying the fourfold-coordinated T_4 sites [33]. Second, deposition of about ~1.0 ML of Ga and subsequent annealing at 300–500°C results in the formation of a set of incommensurate phases, $\gamma(6.3 \times 6.3)$, $\beta(11 \times 11)$ and $\Delta(6.3\sqrt{3} \times 6.3\sqrt{3})$ [27,30,31,34,35]. These incommensurate phases differ in the domain-wall pattern but have a similar atomic arrangement in the interior of the domains, where Ga substitute Si in the outer half of the Si(111) surface bilayer, forming a graphite-like Ga-Si bilayer [30]. Since Ga is a trivalent element, an ideal Ga-Si bilayer would have completely saturated bonding coordination of the Si(111) surface. Developing incommensurate structure is a sequence of the mismatch between the Ga-Si bilayer and the underlying Si(111) substrate lattice.

In the experiment leading to the first observation of SMC, the Ga was deposited onto the Si(111) in two steps rather than one step that was adopted by the previous experiments. First, 1/3 ML of Ga was deposited at room temperature (RT) and then the sample was annealed at 550°C to achieve the $\sqrt{3} \times \sqrt{3}$-Ga reconstructed surface. Second, additional 1/6 ML of Ga was deposited onto the $\sqrt{3} \times \sqrt{3}R30°$ reconstructed surface, and subsequent annealing at 200°C leads to the formation of several species of SMCs [24], as shown by the typical empty-state STM image in Figure 1.

A histogram (Figure 2) of the Ga-induced clusters exhibits four prominent peaks corresponding to four species of similar triangular clusters with n (2, 3, 4, or 5) atoms on their sides. The most abundant species is $n = 4$ clusters, which constitute ~50% of the total number of clusters. The other three species of SMC ($n = 2$, 3 and 5) appear primarily on the boundary of the degenerate $\sqrt{3} \times \sqrt{3}$ domains or areas with increased concentration of defects on the Ga-adatom lattice.

Based on the STM observations and previous XSW studies, atomic models (Figure 3) were proposed for the Ga-SMCs [24] and their validity was supported by density-functional calculations [36]. According to these models, the $n = 4$ SMC, for example (Figure 3c), consists of nine Ga atoms on its periphery, six atop Si-atoms in the interior and a Ga atom at the centre. The most important feature of the model is that the SMCs are essentially made of a Ga-Si bilayer on the Si(111) surface. It is interesting to note that the

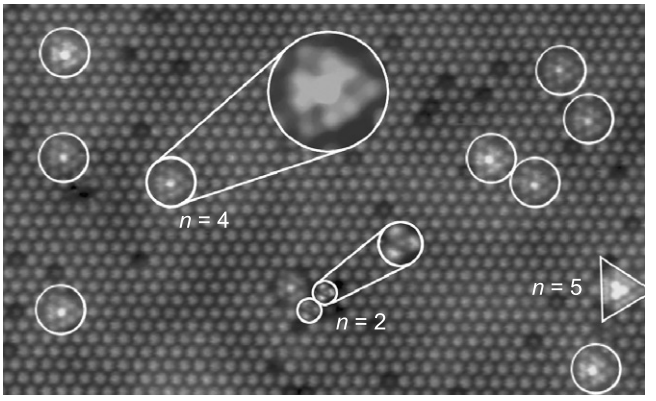

Figure 1. Empty-state (+1.6 V) STM image ($290 \times 165\,\text{Å}^2$) of Ga-induced SMCs on Ga/Si(111)$\sqrt{3} \times \sqrt{3}$ surface. Small and large circles, and triangle indicate $n=2$, $n=4$ and $n=5$ Ga-SMC, respectively. Magnified views of $n=2$ and $n=4$ clusters are also included.

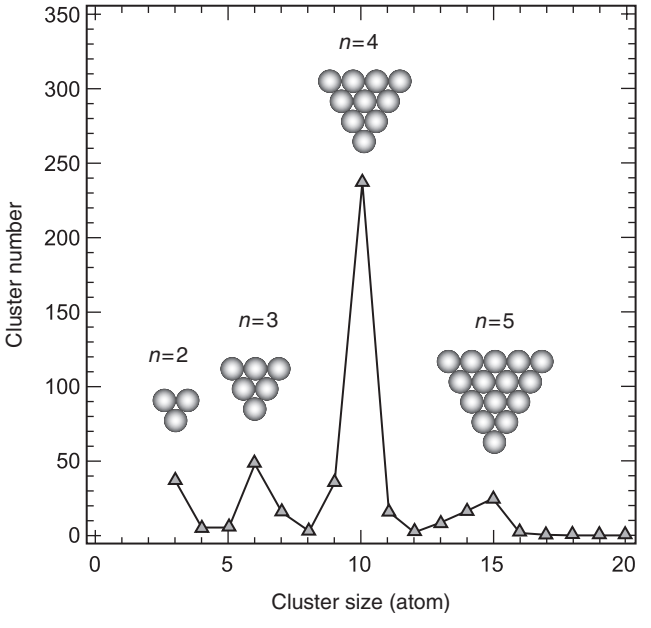

Figure 2. Histogram of Ga-induced clusters on Ga/Si(111)$\sqrt{3} \times \sqrt{3}$ surface showing the existence of magic numbers.

Ga atoms on the periphery have unusual binding configurations: On the inside they are bound to the atop Si atoms, while on the outside they are bound directly to the substrate Si surface. Such an unusual binding configuration for the peripheral Ga atoms is qualitatively consistent with the STM observation that they are only slightly higher than the surrounding Ga adatoms of the $\sqrt{3} \times \sqrt{3}$-Ga reconstruction. The six atop Si atoms in

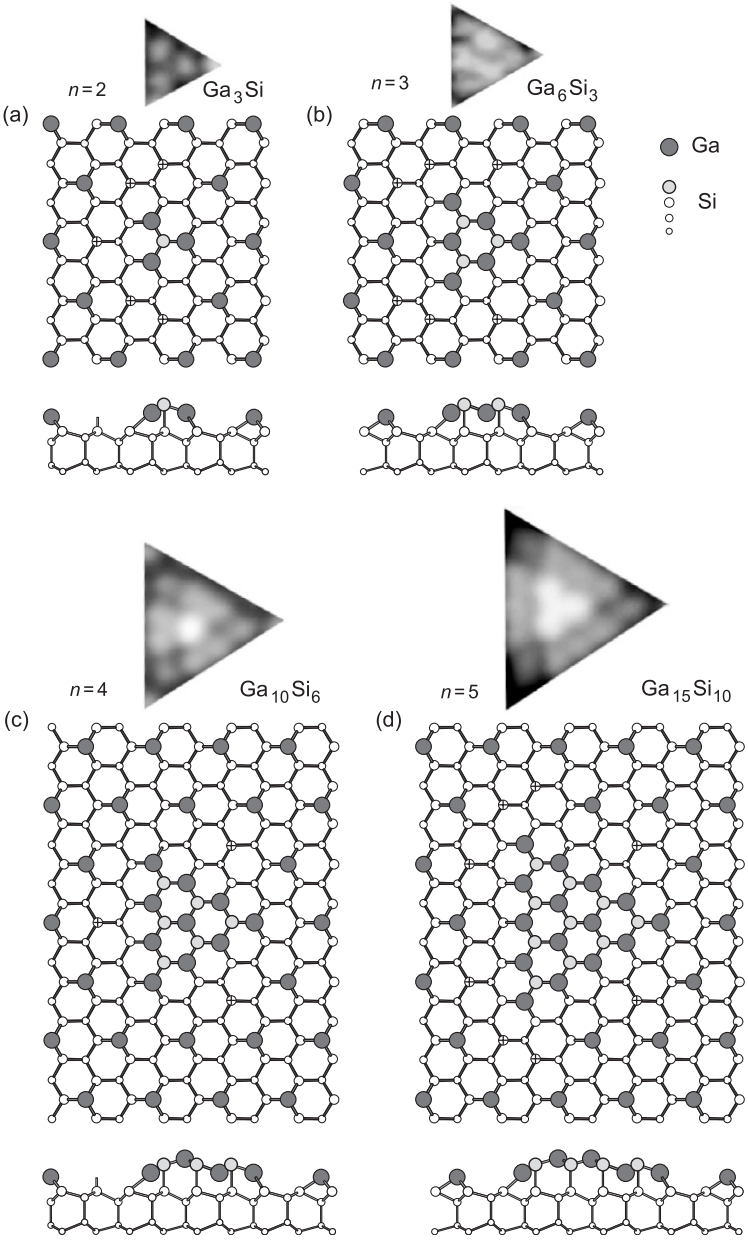

Figure 3. Empty-state STM images and structural models of various surface magic clusters on a $\sqrt{3} \times \sqrt{3}$-reconstructed Ga/Si(111) surface, where n is the number of Ga on each side of a cluster: (a) Ga_3Si cluster ($n = 2$), (b) Ga_6Si_3 cluster ($n = 3$), (c) $Ga_{10}Si_6$ cluster ($n = 4$), (d) $Ga_{15}Si_{10}$ cluster ($n = 5$). Ga atoms are shown by dark grey circles, Si atoms incorporated in the clusters by light grey circles, Si atoms of the Si(111) substrate by white circles. Dangling-bond Si atoms are marked by the crosses.

the cluster interior act as a medium to connect the Ga in the clusters. Although STM observations have never directly revealed these Si, their existence can explain the apparent large distance (~4.1 Å) between neighbouring Ga observed in the STM images as well as the enhanced stability of the cluster [37].

The model for the $n=4$ SMC can be generalized to include the entire family of triangular clusters of different sizes observed in the Ga/Si(111) system. According to the generalized model, the 'stoichiometry' of a SMC with n Ga atoms on its side can be more adequately described by $Ga_{n(n+1)/2}Si_{n(n-1)/2}$. (Hereafter, we will refer to such a metal-induced 'alloy' SMC simply as metal-SMC.) The observed Ga-SMCs (Figure 2) correspond to clusters with $n=2,\ldots,5$. This general formula is adequate even for $n=1$ and ∞. The former corresponds to an individual Ga of the T_4 site of the $\sqrt{3}\times\sqrt{3}$-Ga adatoms surface lattice, while the latter corresponds to an ideal Ga-Si bilayer covering the entire Si(111) surface.

The generalized model also provides a framework for us to understand why $n=4$ SMC are 'more magic' than other magic clusters ($n=2$, 3, and 5) as clearly demonstrated by the cluster size distribution (Figure 2). Simple counting of the number of dangling bonds in the environment of the magic clusters provides a semi-quantitative evaluation of the relative stability of the SMCs with different n. As indicated in Figure 3, the number of dangling bonds is five for the Ga_3Si cluster ($n=2$), six for the Ga_6Si_3 cluster ($n=3$), three for the $Ga_{10}Si_6$ cluster ($n=4$), and eight for the $Ga_{15}Si_{10}$ cluster ($n=5$). The environment of a $n=4$ SMC has a 'closed-shell' structure with the minimum number of dangling bonds, hence it is the most energetically favourable. Simple geometric consideration yields that the surrounding shell is ''closed' when each corner Ga atom of the cluster occupies the site that is originally occupied by Ga-adatoms of the surrounding $\sqrt{3}\times\sqrt{3}$-Ga reconstruction. This takes place for the $n=1,4,7,10,\ldots$ SMCs with the number of dangling bonds $(0,3,6,9,\ldots)$ in their surrounding surface being locally minimized. Note that such geometric 'closure' of the surrounding shell of a SMC does not have a counterpart in the free-space magic clusters because it concerns the bonding satisfaction of the surface atoms neighbouring a cluster rather than that of the cluster itself. It is a kind of concerted self-organization between adsorbed aggregates and its surrounding surface-atoms that allows us to exploit the formation SMC for the growth of identical nanostructures.

It is worth noting that the change in surrounding shell alters the preference for the particular cluster type. The boundaries between the degenerate $\sqrt{3}\times\sqrt{3}$-Ga domains provide such examples. As shown by the STM image and model in Figure 4, the local density of Ga atoms at the domain boundary is reduced, hence many Si atoms have dangling bonds. These vacancies allow $n=2$ and $n=3$ SMCs to 'squeeze' comfortably into some sites reducing or even completely eliminating the number of dangling bonds. This explains why most of the $n=2$ and $n=3$ SMCs are formed at the domain boundaries.

3. Lattices of SMCs

The level of precision and sophistication in our ability to create an ensemble of nanostructures on certain substrates can be divided into three categories. The entry level is to be able to control the type and number of atoms in each and everyone of the nanostructures; second, we need to control the structure of the atoms within a nanostructure as well as its bonding configuration with the underlying substrate surface.

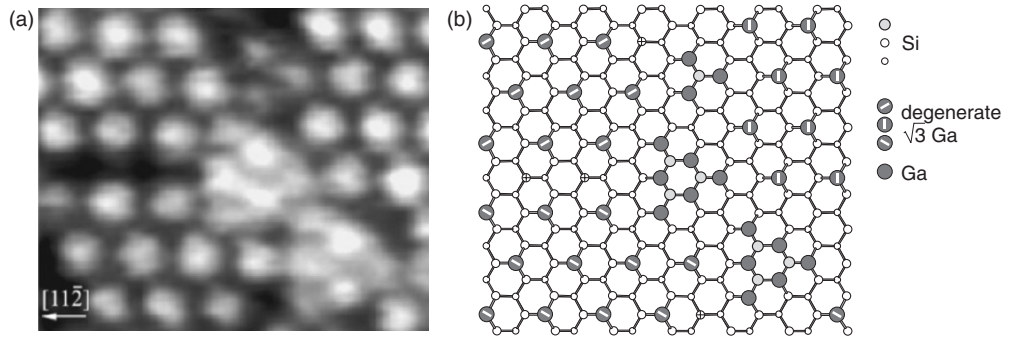

Figure 4. (a) Empty-state (+2.2 V) STM image (54×34 Å^2) and (b) structural model of 2 $n = 3$ and one $n = 2$ Ga-SMCs developed at the boundary between the degenerate domains of the Si(111)$\sqrt{3} \times \sqrt{3}$-Ga adatom lattice [19].

The ultimate level is to be able to precisely arrange an ensemble of identical clusters into a lattice of clusters, whose translational symmetry grantees that constituent clusters have identical surrounding environment. To draw an analogy with chemical synthesis, the first level is equivalent to synthesizing a kind of molecule without any selectivity in its different isomers; second, a kind of molecule with only one type of isomer; and third, a molecular crystal.

Consideration of the random SMC formation leads us to the conclusion that not only the closed-shell atomic arrangement of the cluster itself, but also the closed arrangement of its surrounding shell controls the preference for selecting SMC of a certain type and size. Thus, one could expect to find a surface whose unit cell structure provides conditions for the formation of the SMC with a closed surrounding shell; and their periodic repetition would produce a lattice of SMCs. The Si(111)7×7 surface (Figure 5) seems to be an appealing candidate. In this highly stable surface, the attractive basin inside each 7×7 half unit cell (HUC) is bordered by Si-dimer rows, which act as barriers for the deposited adsorbate atoms. These atoms, if being accumulated in a given HUC up to the required amount, have a chance to build a magic cluster there. This, indeed, has been found for a wide set of adsorbates and to date many examples of the SMC lattice formation are known. However, it should be remarked that the structural perfection of the forming SMC lattices varies in a wide range for various material systems. The most vivid examples of the SMC lattice formation are associated with the Group-III metals, Ga, Al and In, in which case the Me_6Si_3 cluster is nicely built into the 7×7 HUC utilizing Si adatoms already present there and reducing the number of dangling bonds in the HUC from nine to three. We pay these systems special attention by considering their similarities and uniqueness in detail. Other SMC lattices with poorer size and structural uniformity are also reviewed. For example, in the cases of Na, Cu, Tl or Pb on the Si(111)7×7 surface the ordered SMC arrays occupy a limited surface area or coexist with the other cluster species. There are also many adsorbates (e.g., Tl, Ag, Mn, Ge), which being adsorbed onto the Si(111)7×7 surface (typically at a moderate temperature), produce the 7×7 lattice of the shapeless clusters. Interestingly, formation of the SMC lattice are not limited to the template-constrained self-organization of adsorbates on the Si(111)7×7 surface. The cases of the

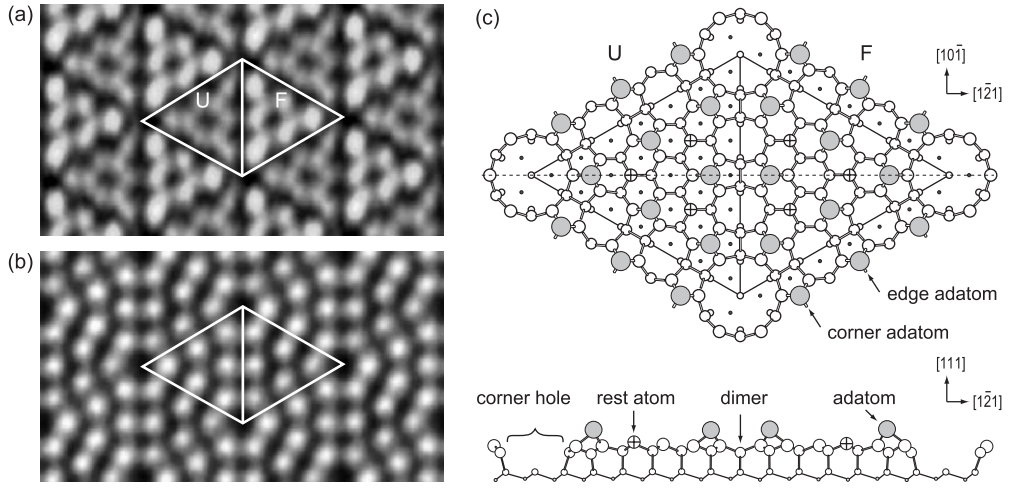

Figure 5. (a) Filled-state (−1.5 V) and (b) empty-state (+2.0 V) STM images of the Si(111)7 × 7 surface with 7 × 7 unit cell being outlined. (b) DAS (dimer-adatom-stacking fault) model by Takayanagi *et al*. [38]. Si adtoms are shown by grey circles, all other Si atoms by smaller white circles. Dangling-bond Si rest-atoms are marked by crosses. Faulted and unfaulted 7 × 7 half unit cells (HUCs) are indicated by F and U, respectively. Note that in the filled-state STM image the faulted-HUCs looks brighter than the unfaulted-HUCs.

so-call ring-clusters on Si(111) and the 4 × 3-In clusters on Si(100) give examples of the SMC lattice formation which is not controlled by a template-constraining effect. Here, the original substrate reconstruction is lifted locally by the SMC formation and the SMC spatial ordering might take place to reduce the number of dangling bonds that are created by the lifting of the original reconstruction.

3.1. *Ga-induced SMC lattice on Si(111)7 × 7*

Deposition of Ga onto a Si(111) 7 × 7 surface at RT results in the formation of various irregular Ga-aggregates, each one of which in most cases is within a 7 × 7 HUC (Figure 6a). Such spontaneous aggregation of adsorbates into separated surface lattice unit cells indicates that the boundaries of the HUCs, which are made of Si dimer rows, act as repulsive barriers for the deposited Ga atoms and the energy landscape on the 7 × 7 surface can effectively distribute the deposited Ga into separate HUCs.

Detailed STM images of the surface revealed that the corner Si-adatoms rarely became part of an irregular Ga-aggregate, only the centre region of a HUC attracts the Ga, consistent with theoretical calculation [39]. Although the calculation did not examine how the energy landscape of a HUC evolves as more and more Ga are added into a HUC, the observation of irregular Ga-aggregates in the centres of the HUCs indicates this energy basin continues to attract Ga even when the region is occupied by an aggregate containing several Ga. Some of the irregular aggregates can even continue to grow across the boundaries of the HUCs, suggesting the interaction between a deposited Ga and an aggregate can either destroy or overcome the repulsive barrier along the boundary a HUC.

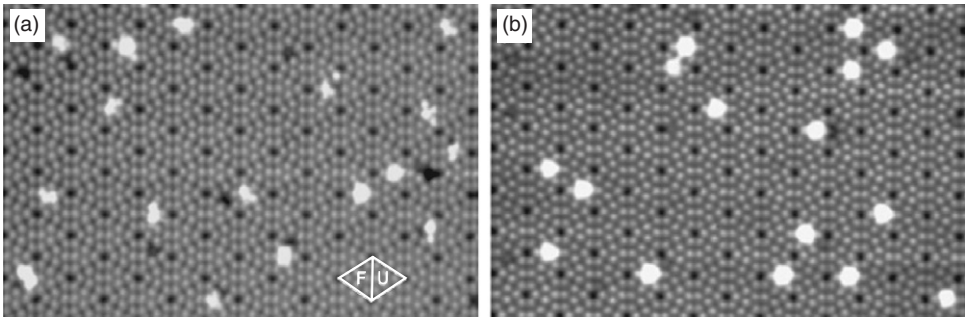

Figure 6. STM images of cluster formation as Ga is deposited on the Si(111)7×7 surface. (a) Clusters prepared at RT have irregular size and shape (0.011 ML of Ga, $V_{\text{sample}} = +2.1$ V). 7×7 unit cell is outlined with indication of the faulted (F) and unfaulted (U) triangular halves. (b) Increased uniformity in the cluster size and shape after 10 seconds of annealing at 300°C (0.017 ML of Ga, $V_{\text{sample}} = -2.2$ V). At such a low coverage, clusters prefer to form on the faulted than unfaulted HUCs with a preference ratio of ~3 : 1.

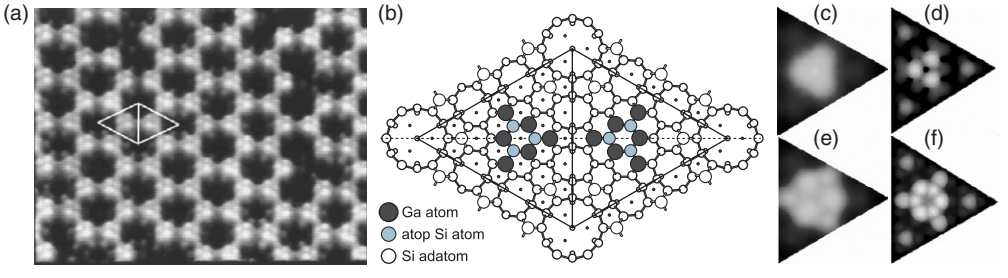

Figure 7. (a) Empty-state (+1.9 V) STM image (190×160 Å^2) of the 2D lattice of Ga-SMCs on the Si(111)7×7surface. (b) Structural model of the Ga_6Si_3 SMCs on the Si(111)7×7 surface. (c), (d) Filled-state (−2.0 V) experimental and calculated images of the Ga_6Si_3 SMC. (e), (f) Empty-state (+2.0 V) experimental and calculated images of the Ga_6Si_3 SMC [44].

Thermal annealing of the sample resulted in significant mass transport of Ga across the repulsive barrier as well as structural reorganization of the clusters. For example, after annealing at 300°C for 10 seconds, the size and shape of the clusters became uniform as shown in Figure 6(b). The observation implies that, at an elevated temperature, small or irregular clusters can disintegrate and the detached species can diffuse across the HUC boundaries to form larger and more stable clusters with certain preferred size/structure. It is interesting to note that, at low coverage, while the irregular clusters formed at RT occupied the two HUCs with approximately equal probability, the SMCs were formed preferentially in the faulted HUCs with ~3 : 1 ratio. The latter implies that the difference in the energy of formation between a SMC on the faulted and unfaulted HUCs is of order ~50 meV.

By depositing ~0.25 ML of Ga onto the Si(111)7×7 surface at ~250 to 350°C, a 2D lattice of SMCs [40–42], as shown in Figure 7(a), was obtained. The clusters occupied both 7×7 HUCs, they had identical size and shape, and each cluster contained six Ga atoms.

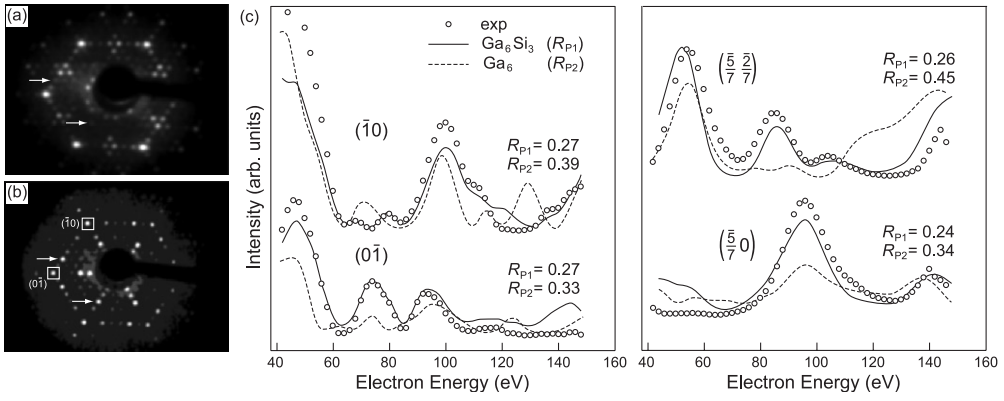

Figure 8. LEED patterns ($E = 60$ eV) of (a) original Si(111)7×7 surface and (b) Ga-induced SMC lattice. (c) Experimental LEED $I - V$ data of the Ga SMC lattice and calculated dynamical LEED spectra of the optimized atomic configurations for the Ga_6Si_3 and Ga_6 models [44].

The Ga-SMC lattice remained stable up to ~400–450°C [40,43], beyond which it irreversibly transformed into the equilibrium phase of $\sqrt{3} \times \sqrt{3}$-Ga reconstruction, which is the global free energy minimum for the material system of Ga/Si(111) at this coverage.

High-resolution STM images of the Ga-SMCs constituting the 2D lattice (Figure 7) are very similar to those of the random Ga_6Si_3 SMCs formed on the Si(111)$\sqrt{3} \times \sqrt{3}$-Ga surface (Figure 3b and Figure 4). This makes the Ga_6Si_3 cluster structure proposed earlier for the random Ga-SMCs to be also a plausible model for the ordered Ga-SMCs (Figure 7b). This model has two appealing features. First, six Ga atoms and three Si atoms form a bonding-satisfied configuration, leading to a reduction in the number of dangling bonds in each HUC from nine to three. (The dangling bonds inside the corner holes are excluded from the counting for simplicity.) This could explain qualitatively the extraordinary stability of the SMCs. Second, three Si atoms adopted by the SMC could originate from the edge Si adatoms of the original Si(111)7×7 HUC and there is no need to look for an unnatural source of Si atoms. The validity of the Ga_6Si_3 model has been proven by first-principles total-energy calculations [41,44], which have shown that the model has the lowest energy among other possible candidates. Simulated STM images of this model demonstrate a good resemblance with the experimental ones (Figure 7(c)–(f)).

Conclusive confirmation of the Ga_6Si_3 model, as well as the first experimental determination of the precise Ga-SMC structure, was obtained using dynamical low energy electron diffraction (LEED) analysis [44]. Note that employment of the advantages of the diffraction method for structural analysis [45] became possible since SMCs with identical size and structure formed an ordered array with exact translational symmetry. Figure 8b shows a LEED pattern acquired under normal-incidence condition from the 2D lattice of Ga-SMCs on Si(111)7×7. At a glance, this LEED pattern is almost identical to the diffraction pattern of the original Si(111)7×7 surface (Figure 8a). However, detailed inspection revealed distinct differences in relative spot intensities at certain beam energies, as indicated by the arrows in Figure 8(a) and (b). The presence of these characteristic

features in the LEED pattern can be used as indicators for the formation of SMC lattice on the Si(111)7 × 7 surface.

For the LEED $I - V$ analysis, a series of LEED patterns of the SMC lattice was captured using beam energies from 40 to 150 eV with an interval of 2 eV and 12 symmetry-inequivalent LEED $I-V$ spectra were recorded. As an example, four experimental $I-V$ spectra are shown in Figure 8(c) together with the calculated spectra of the optimized atomic configurations for two models, the Ga_6Si_3 model and the Ga_6 model (in which three atop Si atoms are missing). A good match between the experimental and calculated spectra is apparent for the Ga_6Si_3model. In contrast, certain peaks of the Ga_6 model are completely out of phase. The Pendry reliability factor R_P is 0.28 for the Ga_6Si_3 model and 0.35 for the Ga_6 model. Therefore, both the reliability factor and the matching of the peak positions support the validity of the Ga_6Si_3 model. The fitting could possibly be improved further if one takes into account partial substitution of the corner Si adatoms, as was done in the RHEED rocking-curve analysis of the Ga-SMC lattice in Ref. [46], where the R_P-factor decreased from 0.21 to 0.14 after 40% of corner Si adatoms in the model were substituted by Ga atoms.

The structure information of the SMC provided by the dynamical LEED experiment and first-principles density-functional calculations is summarized in Table 1. As one can see, the results of the two techniques are quantitatively consistent with each other. The specific bond lengths between any pair of Ga and Si atoms are very close, ranging from 2.4 to 2.5 Å. The atop-Si atoms stand 2.4 Å above the substrate-Si atom. The length of this Si–Si bond is very close to that of the bulk Si–Si bond (2.35 Å), indicating the Ga atoms of a Ga_6Si_3 cluster do not exert too much stress on the atop-Si atoms. Both the edge- and corner-Ga atoms on the peripheral of a Ga_6Si_3 are slightly lower than the atop-Si atoms, with height differences of 0.26 Å and 0.6 Å, respectively. Qualitatively, the result that the edge-Ga atoms are higher than the corner-Ga atoms is consistent with the empty-state STM images.

Table 1. Structure data of III/Si(111)-SMC. D_{e-e} and D_{e-c} represent the distance between two edge-III and between III-edge and III-corner respectively. III(c), III(e), Si(a) are III-corner III-edge, and atop-Si, and d_Z is the height relative to atop-Si.

	Method	D_{e-e} (Å)	D_{e-c}(Å)	Bond	Length (Å)	Atom	d_Z (Å)	Ref.
Ga	Dynamic LEED	4.32	4.21	Ga(c)–Si	2.46, 2.46, 2.50	Ga(c)	−0.60	[44]
				Ga(e)–Si	2.48, 2.48, 2.52	Ga(e)	−0.26	
				Si(a)–Ga	2.48, 2.48, 2.50	Si(a)	0.00	
	ab initio calculations	4.24	4.11	Ga(c)–Si	2.47, 2.47, 2.42	Ga(c)	−0.62	
				Ga(e)–Si	2.44, 2.44, 2.54	Ga(e)	−0.27	
				Si(a)–Ga	2.44, 2.44, 2.42	Si(a)	0.00	
In	*ab initio* calculations	4.61	4.35	In(c)–Si	2.65, 2.65, 2.56	In(c)	−0.58	[41]
				In(e)–Si	2.60, 2.60, 2.69	In(e)	−0.30	
				Si(a)–In	2.60, 2.60, 2.58	Si(a)	0.00	
Al	*ab initio* calculations	4.17	4.19	In(c)–Si	2.49, 2.49, 2.44	In(c)	−0.81	[41]
				In(e)–Si	2.47, 2.47, 2.55	In(e)	−0.27	
				Si(a)–In	2.47, 2.47, 2.44	Si(a)	0.00	

3.2. *Al-induced SMC lattice on Si(111)7 × 7*

Formation of the 2D lattice of Al-induced SMC on Si(111)7 × 7 (Figure 9) was first established independently by Jia *et al*. [41,42,47] and Kotlyar *et al*. [48]. However, a certain indication of Al-SMC formation could be found in the STM images of the so-called α-7 × 7 Al/Si(111) phase acquired earlier by Yoshimura *et al*. [49,50]. Al-SMCs start to form at temperatures above ~250°C, but for the formation of high-quality Al-SMC lattice a typical temperature ranging from ~400 to ~550°C was employed. The SMC lattice formation is completed at ~0.25–0.30 ML of Al, beyond which the system evolves into the Al/Si(111) γ-phase (e.g., see phase diagrams in Refs. [51–53]) through the formation of the intermediate structures [54].

Scanning tunnelling microscopy appearance of the Al-SMC lattice is very similar to that of the Ga-SMC lattice, indicating the similarity of their atomic and electronic structures. Specifically, in the empty-state images the edge-atoms appear brightest and protrusive outwardly in both Al- and Ga-SMC, in sharp contrast to that of the In-SMC to be discussed later. First-principles calculations [42,47] showed that the atomic structure of Al-SMC is indeed very similar to that of the Ga-SMC, and the calculated STM images are also in good agreement with experiment except for the unusually large outward protrusion of the edge-Al observed in the STM image which remains to be understood. The calculated lengths of Al–Si bonds (Table 1) are ~2.5 Å, almost identical to that of Ga-Si, which could be explained by the similar covalent radii of Al and Ga. Among the Group-III metal-SMCs, the Al-SMCs have the best uniformity, ordering, and thermal stability. These unique properties could be the reason why most of the recent publications on the Al-SMCs were devoted either to studying the formation mechanisms of the Al-SMC lattice [48, 54, 55] or its stability at elevated temperatures [41,42,48,56,57].

The formation kinetics of the Al-SMC lattice exhibit many interesting features. There are three types of adsorption site for an Al adatom. First, it can be incorporated in SMC (there are 12 such sites per 7 × 7 unit cell). Second, it can replace a corner Si adatom (six sites per 7 × 7 unit cell). Third, it can substitute in for an edge Si adatom, if the HUC does not contain a SMC (six sites per 7 × 7 unit cell). Variation in the occupation number

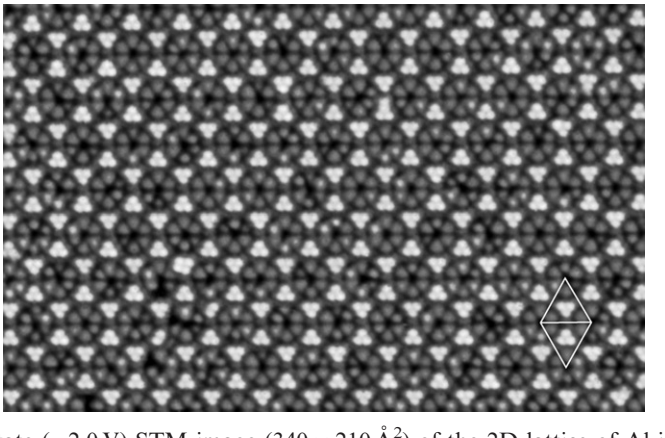

Figure 9. Filled-state (−2.0 V) STM image (340 × 210 Å^2) of the 2D lattice of Al-induced SMC on Si(111)7 × 7 surface.

for each site in the course of Al deposition is illustrated in Figure 10. One can see that up to ~0.06–0.08 ML (i.e., at the stage marked as stage I in Figure 10), SMC formation does not occur, and the major process is the substitution of the edge and corner Si-adatoms of the Si(111)7 × 7 surface. The displaced Si atoms aggregate to form 7 × 7 islands or incorporate into the step edges. In stage II (from ~3 to ~10 Al atoms per 7 × 7 unit cell, i.e., at ~0.06–0.20 ML of Al), SMC formation becomes a dominant process and its density grows linearly with Al coverage (see Figure 10(a)).

The main source of Si atoms for the formation of a SMC, which requires three Si atoms, is the edge Si-adatoms. At the end of stage II, about 75% of the 7 × 7 HUCs are occupied by SMCs. As the coverage goes beyond 0.20 ML (stage III in Figure 10), the edge Si-adatoms are no longer available for the formation of SMCs, therefore the Si atoms are mostly supplied by the corner Si-adatoms that has been substituted by Al. As a result, the density of Al on the corner sites increases rapidly, and eventually about half of the corner Si sites become occupied by Al (see Figure 11). According to the estimation extracted from the published data, the density of Al occupying the corner sites increases with the formation temperature. For temperatures around 300, 400, and 500°C, there are ~2.0 [42], ~2.7 [55], and ~3.3 [48] Al atoms per 7 × 7 unit cell, respectively. Similar to Al,

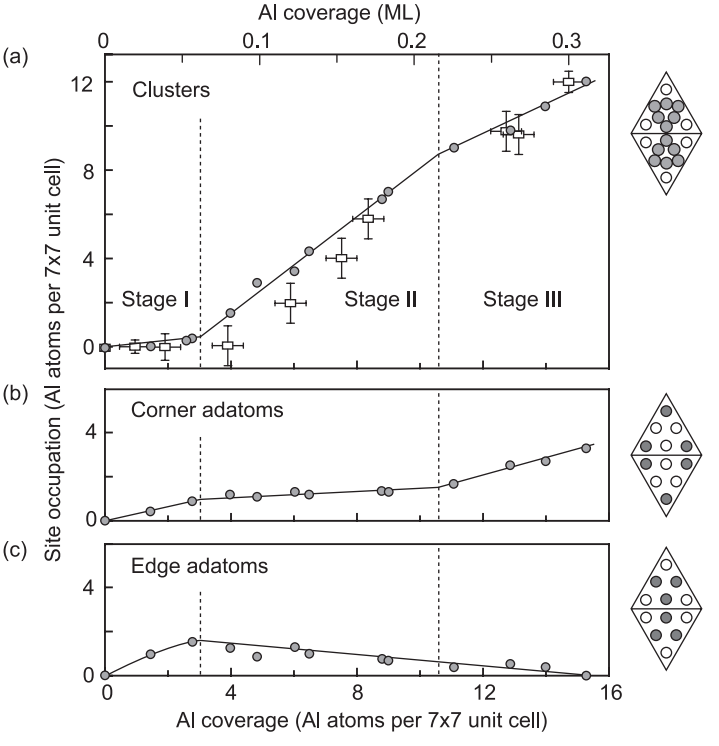

Figure 10. Occupation of the three adsorption sites: (a) in the magic clusters; (b) in the edge adatom sites; and (c) in the corner adatom sites, as a function of deposited Al coverage. The data from Ref. [48] are shown by the grey circles, the data from Ref. [55] are shown by the open squares with the error bars. Location of the adsorption sites within a 7 × 7 unit cell is illustrated schematically at the right side of the figure.

substitution of the corner Si-adatoms has also been observed in the formation of Ga- [46] and In-SMC lattices [58]. Specifically, the combination of RHEED analysis and STM observations enabled the authors of Ref. [46] to conclude that ~40% of the corner Si-adatoms (i.e., ~2.4 atoms per 7×7 unit cell) are replaced by Ga atoms.

A lattice of Al-SMCs remains stable up to ~500–600°C. It transforms into the $\sqrt{3} \times \sqrt{3}$-Al surface with inclusions of the $\sqrt{7} \times \sqrt{7}$-Al phase at higher temperatures [41,48]. High-temperature STM observations [56,57] have revealed that the disintegration of the Al-SMCs into Al adatoms becomes noticeable at the time scale of the STM observation starting from ~400°C. However, at temperatures of ~400–500°C formation of the $\sqrt{3} \times \sqrt{3}$-Al phase is not possible, since it requires disruption of the stable 7×7 DAS structure. Hence, condensation of the released Al adatoms into the new clusters should also occur. This has been directly observed at the incomplete Al-SMC lattice, where a certain portion of clusters randomly change their positions in the course of STM observation. At temperatures around ~550°C, disruption of the 7×7 surface and formation of the $\sqrt{3} \times \sqrt{3}$-Al phase becomes possible. The triangular domains of the $\sqrt{3} \times \sqrt{3}$-Al phase develop first near the up-step edges on the terraces and propagate further onto the terraces accumulating Al adatoms supplied by the disintegrated Al-SMCs.

3.3. *In-induced SMC lattice on Si(111)7 × 7*

Though the In-induced SMCs on the Si(111) surface have a Me_6Si_3 atomic structure [41, 59] similar to that of the Ga- and Al-induced SMCs, there are some peculiar features occurring only in this particular material system. These are (i) the lowest formation temperature, and consequently the lowest thermal stability [41,58–60], (ii) the ability to form two types of SMC lattice at ~0.12 ML and ~0.24 ML [41,59] and (iii) qualitatively different STM images of the In-SMC [41,59].

Formation of the ordered In-SMC lattice takes place in the relatively narrow temperature interval from ~100 and ~200°C [41,59]. If the substrate is held at lower temperatures, say, at RT, a disordered featureless surface appears [61,62]. Growth at higher temperatures results in the formation of a more stable $\sqrt{3} \times \sqrt{3}$-In reconstruction.

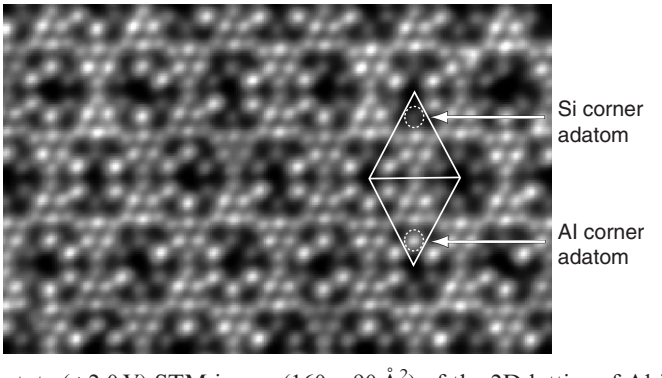

Figure 11. Empty-state (+2.0 V) STM image (160×90 Å^2) of the 2D lattice of Al-induced SMC on Si(111)7×7 surface with the corner Si adatoms partially substituted by Al atoms. Compared to Si adatoms, Al atoms have a brighter STM contrast. The 7×7 unit cell is outlined.

Though for the preparation of the Si(111)$\sqrt{3} \times \sqrt{3}$-In surface the temperatures of ~400–550°C are typically used [63], disintegration of the In-induced SMCs and transformation of the surface into the $\sqrt{3} \times \sqrt{3}$-In phase already starts at ~300°C (the process of In-SMC lattice disintegration upon annealing is considered in detail in Ref. [58]).

The two HUCs of the 7 × 7-reconstructed Si(111) surface are different both structurally and electronically. The structural difference resides most prominently in the height of adatoms: in the faulted HUC they are ~0.1–0.2 Å higher than those in the unfaulted HUC [65–67]. The electronic difference manifests itself in the different STM contrast of the adatoms in the two HUCs. While in the empty-state STM image (Figure 5b) the adatoms in the two HUCs look almost identical, in the filled-state STM image (Figure 5a) the ones in faulted HUC appear noticeably brighter and higher by ~0.3–0.4 Å. Consequently, the potential surface of the adsorption wells in the two HUCs differs in both the barrier height and depth [68,69]. The wells in the faulted HUC are typically deeper, though the particular energy difference depends on the type of the adsorbate. For indium, the difference is quite evident. Starting from low In coverage, the In-SMCs prefer to form on the faulted HUCs, as shown in Figure 12(a). For example, after deposition of ~0.05 ML of In, 92% of clusters occupy the faulted HUCs and only 8% the unfaulted HUCs [41]. Applying the Boltzmann distribution to this result, one obtains the adsorption energy difference between the two halves to be 0.08 eV, which agrees with the results of the first-principles calculations, 0.1 eV/cluster [41]. Remarkably, the preference remains up to ~0.12 ML, where almost all faulted HUCs become occupied by the In-SMCs and the

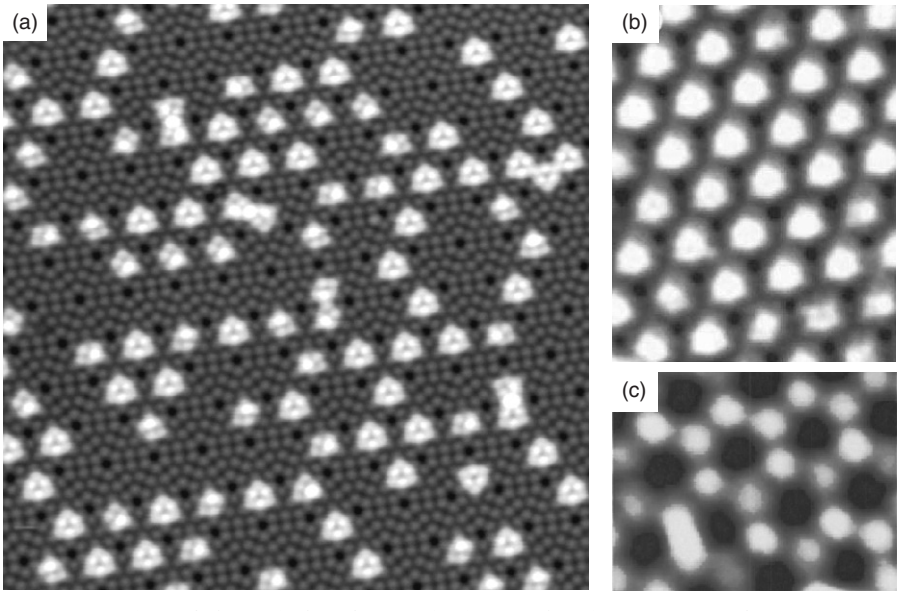

Figure 12. Formation of the In-induced SMC lattice on the Si(111)7 × 7 surface. (a) Empty-state (+1.3 V) STM image (55 × 55 Å^2) after depositing ~0.09 ML of In at 200°C. (b) STM image of the 'half-covered' In-SMC lattice at ~0.12 ML of In [59]. (c) STM image of the 'full-covered' In-SMC lattice at ~0.20 ML of In [41].

so-called 'half-covered' SMC 7×7 lattice is formed (Figure 12b). This behaviour is in contrast to that of the Ga- and Al-SMCs, as illustrated by Figure 13, which summarizes the data from various publications concerning the preference of the Group-III-SMCs to occupy the faulted HUCs. For the In-SMCs the preference is always the highest and remain as high as ~0.85 at the point of the 'half-covered lattice' (i.e., one cluster per unit cell), while for the Al-SMCs the preference is relatively high (albeit still smaller than for In-SMCs) only at low cluster density and vanishes with increasing density. At the 'half-covered-lattice' point, the preference is ~0.5–0.6 (i.e., the faulted and unfaulted HUCs are occupied almost equally). For the Ga-SMCs, the preference is observed only in the low coverage range in a subtle fashion.

With increasing In coverage beyond 0.12 ML, the In-SMCs begin to occupy the unfaulted HUCs of the Si(111)7×7 surface. These clusters in the unfaulted HUCs have a similar STM appearance to those in the faulted HUCs. At ~0.24 ML of In, all HUCs become occupied by the In-SMCs and the 'full-covered' lattice exhibits a characteristic honeycomb structure (Figure 12c) similar to that observed in the case of Ga- and Al-SMCs.

In the high-resolution STM images (especially the ones taken at low bias voltages), the In-SMCs appear different from those of the Ga- and Al-SMCs. While in the empty-state images of the Ga- and Al-SMCs, the edge protrusions always appear brighter than the corner protrusions (see, for example, Figure 7), the appearances are reversed: the corner protrusions are brighter than the edge ones (see Figure 14). Interestingly, the corner In atoms of a In-SMC are actually ~0.3 Å lower than the edge In atoms, as revealed by the

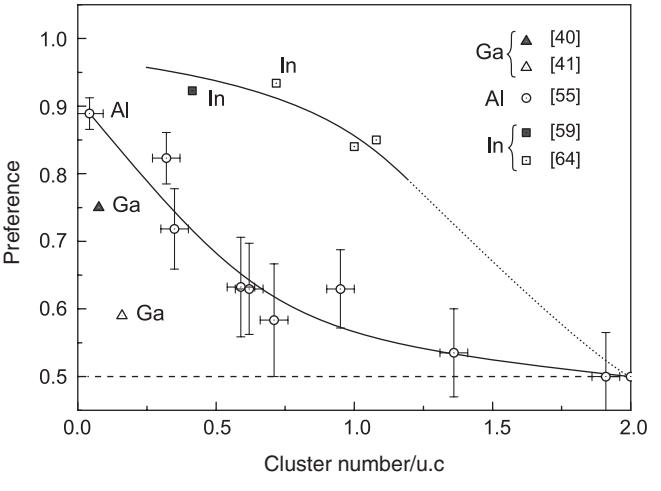

Figure 13. Preference for the Group-III SMC occupation of the faulted HUCs on Si(111)7×7 surface as a function of the cluster density. (Preference shows the ratio of the number of SMCs in the faulted HUC to the total number of SMCs. Preference of 1.0 corresponds to the ideal case, when exclusively faulted HUCs are occupied by SMCs; preference of 0.5 to the equal population of both faulted and unfaulted HUCs.) Cluster density is expressed in the number of clusters per 7×7 unit cell, thus 1.0 corresponds to the 'half-covered' lattice at 0.12 ML, and 2.0 to the 'full-covered' lattice at 0.24 ML. The data for In are shown by squares, for Al by circles and for Ga by triangles. The source references for the particular data are indicated in the right top corner of the figure.

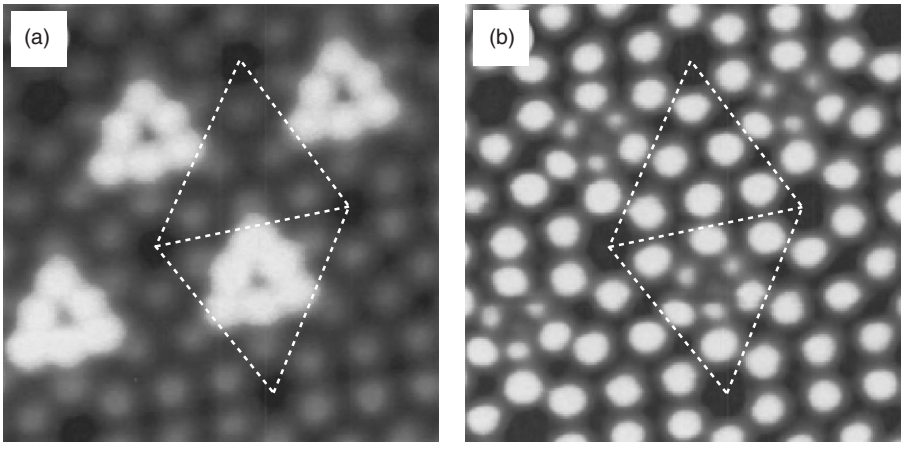

Figure 14. Empty-state atomically resolved STM images ($55 \times 55\,\text{Å}^2$) from the same area with In-SMCs on Si(111)7×7 at bias voltage of (a) $+0.6$ V and (b) $+0.2$ V [41].

first-principles calculations [41] (see Table 1). Jia *et al*. [41] argued that the difference in STM appearance stems from the difference in the bonding configurations of corner group-III-atoms in the different SMCs: the average bond angle of the In corner atom (104.6°) is smaller than the 109.5°-tetrahedral angle leading to the sp^3-like bonding, while the average bond angles of the Ga and Al corner atoms (110.7° and 112.7°, respectively) are larger than 109.5° resulting in the sp^2-like bonding.

3.4. *In-induced 4 × 3 SMC lattice on Si(100)*

An atomically-clean Si(100)2×1 surface is known to be covered by Si-dimers arranged into rows. In comparison with the Si(111)7×7 surface, it has shorter periodicity, smaller corrugation amplitude, and lower stability. Due to these properties, the Si(100)2×1 surface is not expected to produce a strong template effect on the growth of nanostructures. Hence, intuitively, it does not seem to be a suitable substrate for achieving a lattice of SMCs. So, it is especially remarkable that, in fact, adsorption of In (and to a certain extent of Al) results in the formation of the high-quality 2D lattice of the identical SMCs. In contrast to the above discussed cases of the 2D SMC lattices on the Si(111)7×7 surface, here the spatial ordering of SMCs is not controlled by the template constraining effect from the substrate. The initial Si(100)2×1 substrate reconstruction is lifted and SMC ordering is a result of self-assembly.

Before discussing the SMC growth, we would like to recall that, in the low-temperature range (from RT to about 350°C) and metal coverage below 0.5 ML, Al, In and Ga demonstrate a very similar behaviour, namely, upon metal adsorption substrate Si-dimers are preserved, while metal adatoms form symmetric dimers located in the troughs between Si-dimer rows and oriented parallel to the Si-dimers [70]. Thus, under the above conditions no adsorbate clusters other than dimers are formed. Therefore, our prime interest concerns the growth at elevated temperatures.

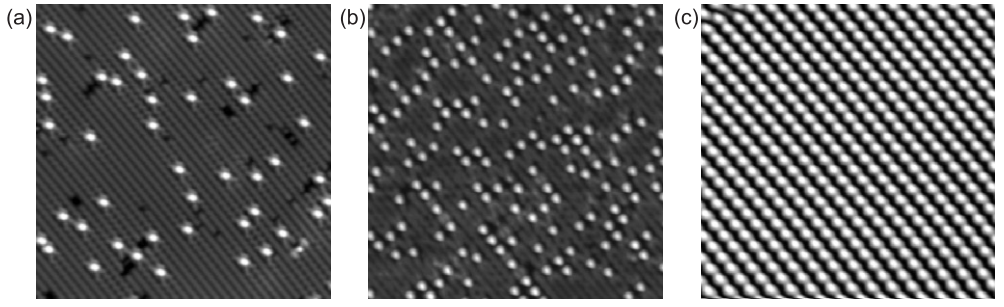

Figure 15. $290 \times 290\,\text{Å}^2$ filled-state (-1.8 V) STM images of the In/Si(100) surface formed upon adsorption of (a) 0.05 ML and (b) 0.18 ML and (c) 0.50 ML of In at 500°C. In/Si(100) SMCs (seen as the bright round protrusions) are distributed randomly at low coverages, but become aligned into the well-ordered 4×3 superlattice at saturating coverage.

Formation of the submonolayer In/Si(100) interface at about 500°C furnishes the most vivid example of the ordered nanoclustering. Starting from the very low In coverage of a few percent of monolayer, identical-size SMCs are formed (Figure 15a). Spatial distribution of the forming clusters is random. With increasing In coverage, the number density of clusters increases, but their spatial distribution still remains almost random [71, 72]. This is clearly seen in Figure 15(b), which shows the Si(100)2×1 surface after deposition of ~0.18 ML of In at 500°C. Though scarce local ordering of SMCs occurs occasionally, a long-range ordering is apparently lacking. The SMCs self-organize into the well-ordered 4×3 superlattice [71,72] only when the saturation In coverage of 0.5 ML is attained (Figure 15c).

These observations indicate that the formation of the Si(100)4×3-In surface is qualitatively different from the other metal-induced silicon reconstructions. Domains of the reconstructions usually nucleate at the step edges or the defect sites, when the local adsorbate coverage reaches a certain critical value. With increasing coverage, the domains grow in size until they touch each other and the whole surface becomes occupied by a given reconstruction. Even at the very early stages of the reconstruction, each domain contains several unit cells suggesting that the reconstruction is a result of the collective effect of all the adsorbates inside the domain. In contrast, the 4×3-In unit cell is essentially a SMC, which can occur both as a single cluster, as well as a building block of the extended 2D lattice of SMCs.

The atomic structure of the Si(100)4×3-In surface was a subject of furious debates for many years, until the structural model proposed by Bunk *et al*. [73] was accepted as conclusive. The model is supported by most of the recent studies using various experimental and theoretical techniques, including X-ray diffraction [73,74], photoelectron diffraction [75], photoelectron holography [76], first-principles total-energy calculations [77–79] and STM image simulations [78,80]. According to the model, six In atoms and seven Si atoms form a stable pyramid-like In_6Si_7 cluster, as shown in Figure 16.

As for the other Group-III adsorbates, aluminium is the second metal, exhibiting a tendency towards SMC formation on the Si(100) surface. Moreover, the bias-dependent STM appearance of the Al- and In-SMCs appears to be very similar. As shown in Table 2,

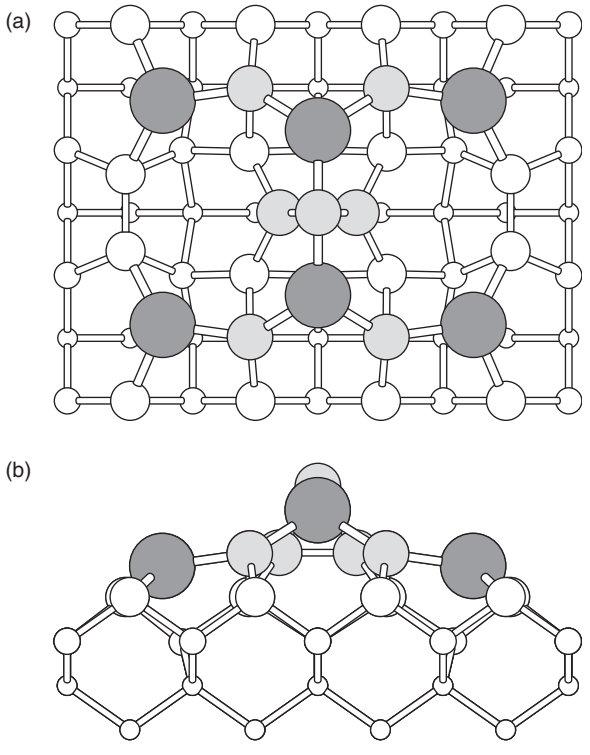

Figure 16. (a) Top view and (b) side view of the atomic structure of the SMC formed by group III metals, In and Al, on Si(100), as proposed by Bunk *et al.* [73]. The most of the recent experimental and theoretical studies support this structural model, in which six metal atoms (shown by dark-grey circles) and seven Si atoms (shown by light-grey circles) form a pyramid-like In_6Si_7 cluster occupying $4a \times 3a$ area.

Table 2. $40 \times 40\,\text{Å}^2$ STM images of Al and In nanoclusters acquired at various bias voltages.

Metal	Sample bias voltage			
	2:0 V	+1:0 V	+2:0 V	
In	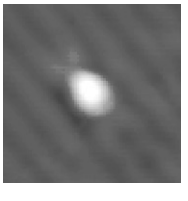	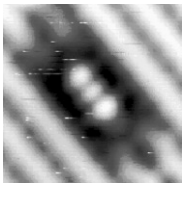	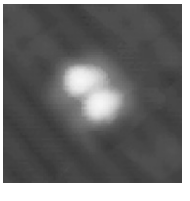	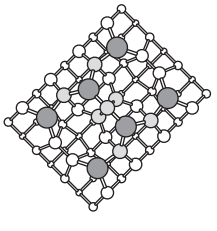
Al	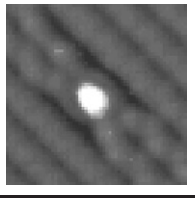	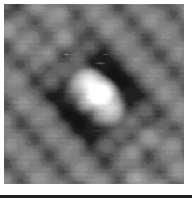	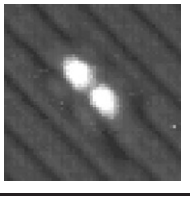	

both clusters show up as a single round protrusion in the filled-state images, as three oval protrusions in the empty-state images at about +1.0 V sample bias and as a pair of oval protrusions in the empty-state images at about +2.0 V. Results of the first-principles total-energy calculations [79,81,82], STM image simulation [81], and ion scattering spectroscopy analysis [83] have also confirmed the structural similarity of the In- and Al-SMCs on Si(100). Both are described by Bunk's model.

However, the tendency for clustering in the case of the Al/Si(100) system is not as unambiguous as that for In/Si(100). It has been found [84] that cluster formation is not a unique way for Al interaction with a heated Si(100)2×1 surface. In fact, there are two competitive mechanisms. Besides nanocluster formation, substitutional incorporation of Al atoms into the top Si(100) substrate layer takes place, which becomes especially pronounced in the presence of the missing-dimer defects. Competition between the two mechanisms and the relatively low mobility of Al adatoms on Si(100) result in poor ordering of the Al/Si(100) SMCs into the 2D lattice. They form restricted domains with a 4×5 periodicity [85].

Deposition of Ga at low temperatures behaved very similar to that of In and Al. Moreover, the total-energy calculations [79] suggest that a Ga cluster based on Bunk's structural model (Figure 16) is stable. However, in the experiments using RT deposition of 0.1–0.5 ML of Ga followed by annealing to ~600°C or direct Ga deposition onto the Si(100) heated to the same temperatures, no indication of SMC formation was detected. Instead, Ga atoms were found to displace Si atoms and form arrays of Ga dimers embedded into the top Si(100) substrate layer [85].

No indication on the nanoclustering has been found also in the Tl/Si(100) system. Upon the adsorption in the temperature range from RT to about 250°C Tl forms a number of reconstructions with 2×2 and 2×1 periodicity and leaves the underlying Si(100)2×1 substrate almost intact [86,87]. Since thallium atoms are weakly bonded to the Si(100) substrate, they are highly mobile and desorb from the surface at temperatures above 270°C.

The results of the tests for the formation of SMCs induced by the adsorption of Group-III metals on the Si(100) surface are summarized in Table 3. It appears that the tendency for the clustering process competes with the tendency for the substitutional adsorption, i.e., displacement of Si atoms and formation of the metal dimers embedded into the top Si(100) substrate layer. The outcome of the competition seemed to correlate with the covalent radius of the adsorbate provided its interaction with the substrate is strong enough. For elements with larger covalent radii, the clustering process prevailed while for those with smaller radii, the substitutional adsorption dominates. Considering the cases of Al, In, and Ga, which interact strongly with the Si(100)

Table 3. Ability of group III metals to form magic clusters on Si(100) as a function of metal covalent radius.

Metal	Covalent radius, Å	Magic clusters	Substitutional dimers
Ga	1.22	NO	YES
Al	1.43	YES	YES
In	1.63	YES	NO
Tl	1.70	NO	NO

substrate, In has the largest covalent radius (1.63 Å) and demonstrates the most definitive tendency to form ordered nanoclusters. Aluminium has a medium covalent radius (1.43 Å) and exhibits both clustering and substitutional adsorption. Gallium has the smallest covalent radius (1.22 Å) and displays only substitutional adsorption. The examples of In and Al SMC formation suggest that the cluster formation involves considerable atomic rearrangement within the top Si substrate layer, which is possible only with the strong adsorbate–substrate interaction. Although Tl has a covalent radius (1.70 Å) close to that of In, its weak interaction with the substrate seems to prevent it from clustering or substitutional adsorption. As a final remark on the SMC formation induced by the adsorption of group III elements on Si(111), adsorption of ~1 ML of Ga and Al is known to induce Si(100)$8 \times n$-Ga [88–90] and Si(100)c(4×12)-Al [91–93] reconstructions, respectively, which might be thought of as ordered SMC arrays by some researchers. However, we believe that these structures belong to the class of the ordinary metal-induced reconstructions since they only occurred in the form of the ordered arrays, but not as isolated clusters.

4. Ordered SMC arrays

In this section we consider the systems in which the array of clusters does not have sufficient structural quality to be treated as a lattice of SMCs. These are partially ordered arrays with obvious imperfections in the limited surface areas occupied by the ordered SMC array or arrays with simultaneous presence of various types of clusters.

4.1. *Na- and K-induced SMCs on Si(111)7 × 7*

The relatively weak bonding and high mobility of Na on the Si(111) surface lead to an interesting scenario for the formation of the Na-SMC lattice on Si(111)7×7 surface at RT [94–97]. Below the critical coverage of ~0.08 ML, SMC formation did not take place (Figure 17), and no sign of the Na adsorbates other than contrast modulation coupled with streaky noise could be found in the STM images (Figure 18). However, the marked work function drop (Figure 17) and development of new features in the photoelectron spectra [95] clearly indicated that Na atoms were present on the surface. First-principles total-energy calculations [94,98] showed that adsorption of a Na atom on neither the Si adatom site nor the Si rest-atom site is favourable. The 12 lowest energy sites are located around the Si rest atoms, forming a circular 'basin' [39,99,100]. The diffusion of a Na atom within the basin is characterized by an energy barrier of 0.14 eV, while the diffusion barriers for hopping among the three neighbouring basins within the 7×7 HUC and crossing the unit cell boundary is 0.36 and 0.42 eV, respectively. At RT, motions of all the tree types are activated and Na atoms move faster than the typical STM scan speed. In addition, it has been found that the Na atom transfers a charge to the nearest Si adatom, making it brighter in the filled-state STM images. As the faulted 7×7 HUC is more favourable than the unfaulted one by 0.06 eV, the Na atom stays longer in the faulted half, making it even brighter in the filled-state STM images. These results of calculations can account for all of the specific features in the STM images (Figure 18).

The clustering induced by Na adsorption became observable starting from ~0.08 ML, i.e., ~4 atoms per 7×7 unit cell (Figure 19) and their number density increased

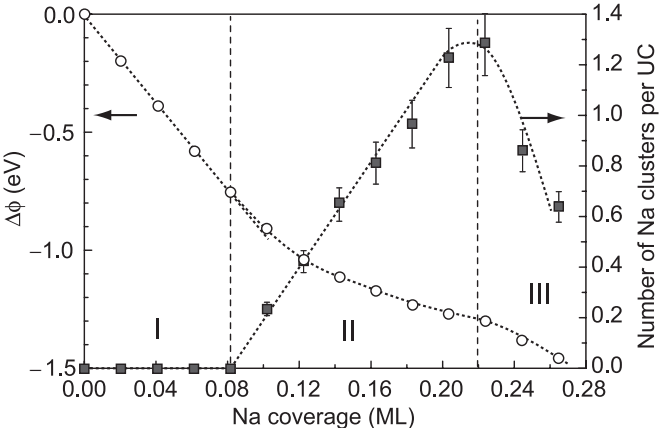

Figure 17. Change of the surface work function ($\Delta\phi$) [white circles; left scale] and the number of Na clusters per unit cell [grey squares; right scale] as a function of Na coverage. Two inflection points are clearly evident at 0.08 and 0.22 ML, dividing into the three distinctly different adsorption stages: (I) a gas-like phase; (II) formation of Na clusters; and (III) decay of clusters [94].

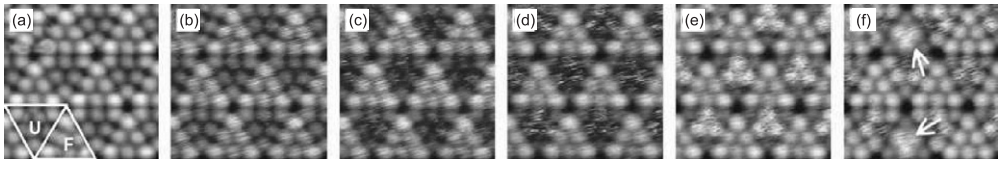

Figure 18. Filled-state (−1.3 V) STM images of the Si(111)7 × 7 surface with Na coverage at (a) 0, (b) 0.02, (c) 0.04, (e) 0.08 and (f) 0.10 ML. In (a) a 7 × 7 unit cell is outlined with faulted unit cell half marked by F and unfaulted half by U [94].

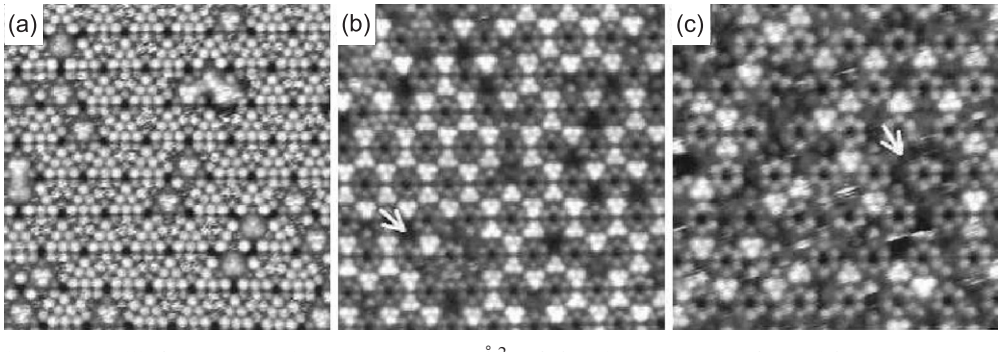

Figure 19. Filled-state STM images (200 × 200 Å^2) of the Si(111)7 × 7 surface with Na coverage at (a) 0.10, (b) 0.22, and (c) 0.26 ML. (a) and (b) illustrates the formation of Na-SMCs and (c) their decay (marked by arrows) [96].

monotonically with Na coverage (Figure 17). The slope of the curve indicated that each cluster contained six Na atoms. For the atomic structure of the Na-SMC, two models have been proposed, the hexagon model and the trimer model [97]. In the hexagon model, six Na atoms form a hexagon in the centre of the 7×7 HUC, keeping all Si adatoms in their original configuration. In the trimer model, three edge Si adatoms move inward to form a trimer with a bond length of 2.44 Å and six Na atoms form a triangle centred at this trimer. One of the corner Na atom is pushed outwards, resulting in the triply-degenerate mirror symmetry structure (the other two states can be obtained by 120° rotation). In comparison to the hexagon model, the trimer model is energetically more favourable but by only 0.02 eV/atom [97]. The simulated STM images of the trimer model (averaged over the degenerate states) reproduce the experimental images noticeably better.

At ~0.22 ML of Na, the maximum density of the Na-SMCs was attained, which appeared to have 1.3 clusters per 7×7 unit cell rather than two expected for a perfect lattice. At higher Na coverages, the density of the Na-SMCs decreased and disordered features appeared, indicating that the clusters became irregular due to additional Na atoms. One can see in Figure 17 that such structural transformations are reflected in the change of the work function, which displays a fast drop (associated with a charge transfer from Na atoms to Si substrate) when the gas-like Na-adatom phase develops on the surface. The decrease in the work function slows down when Na-SMC formation takes place and accelerates again when the number of Na-SMC reduces.

The ability of other alkali metals, Li, K and Cs, to form SMC arrays has been explored in Refs. [96,97,101,102]. The atomic size effect (i.e., larger atoms have weaker interaction with the substrate and therefore higher mobility) was found to play an essential role in adsorption and clustering of alkali metals. Lithium, the lightest one among the alkali metals, demonstrates the classical adsorption behaviour with the formation of clusters from the beginning of the deposition. However, Li-SMC formation has not been reported. Potassium behaves similar to Na except for its higher mobility. Below ~0.08 ML, K forms a two-dimensional gas of adatoms, whose migration speed was so fast that it produced noise-free STM images. (Another difference is that K transfers more charge to the substrate than Na.) Above ~0.08 ML, K-SMCs were formed, which occupied only the faulted 7×7 unit cell halves, leaving the unfaulted halves completely empty (Figure 20a). The number of K atoms in each SMC derived from the slope of the dependence of cluster number density on K coverage was 6, the same as in the Na-SMC. However, their structures were apparently different. Moreover, two types of K-SMC have been detected (Figure 20b–d), of which one can occur in three equivalent orientations with two different chiralities and the second one in three orientations, thus there are in total nine possible configurations of K clusters. It is remarkable that at RT K clusters were observed to jump inside the 7×7 HUC among these nine configurations (along well-defined routes), and some clusters disappeared while the other new ones appeared during STM tip scanning. As for Cs, it also formed 2D adatom gas at low coverages and clusters at higher coverages, but the Cs-clusters were irregular and no SMC was observed.

4.2. *Cu-induced SMCs on Si(111)7 × 7*

When submonolayers of Cu (e.g., ~0.1–0.4 ML of Cu) were deposited onto a Si(111)7×7 substrate at RT, ordered arrays of SMCs were formed at the surface. Cluster formation

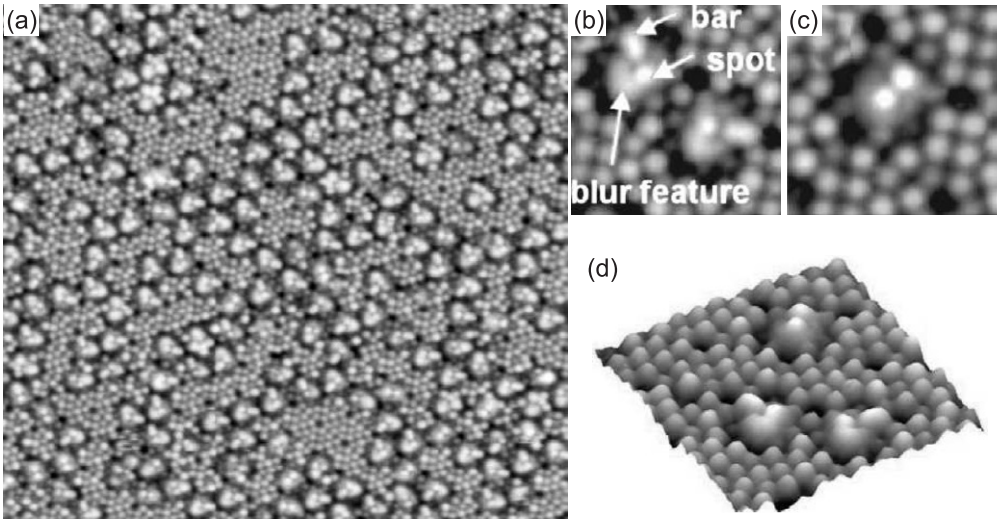

Figure 20. (a) Filled-state (−1.6 V) STM image (500×500 Å^2) of K-SMCs on the Si(111)7×7 surface; (b) and (c) are zoom-in images of the two types of K-SMCs. (d) 3D image of an area with clusters of the both types [96].

was first detected by STM in the 1990s [103,104], but only recently have these clusters been designated as SMCs [105,106]. At low Cu coverages (up to ~0.1 ML), Cu-SMCs occupy preferentially the faulted 7×7 HUCs, resulting in a 'half-covered' SMC ordered array [105]. At the higher Cu coverages, Cu-SMC occupy both faulted and unfaulted HUCs and result in a 'full-covered' SMC ordered array in a local area, as shown in Figure 21(a). The range of the translational order in the Cu-SMC arrays is much shorter than that of the arrays formed on Si(111)7×7 by Ga, Al and In. It is usually destroyed by the presence of random clusters with irregular shape.

The Cu-SMC has some distinct features that were revealed by the high-resolution STM images (Figure 21b) acquired at various bias voltages. The contrast of the clusters varied dramatically with the variation of the bias voltage, suggesting that the clusters are not composed of only Cu atoms but rather of both Cu and Si atoms. Most interestingly, the images of a Cu-SMC situated in the faulted and unfaulted 7×7 HUCs appeared essentially identical at some sample voltages (−1.0 V, −0.5 V, +0.5 V, +2.0 V) but drastically different at others (+1.0 V, +1.5 V). Since such a dramatic dependence of the cluster image on its location (faulted or unfaulted) has never been observed in other known SMCs, it is likely that the Cu-SMC has a different atomic structure, which remains to be determined quantitatively.

4.3. *Co- and Ni-induced SMCs (ring-clusters) on Si(111)*

High-temperature deposition of many silicide-forming metals (e.g., Ni [107–113], Co [109,114–116], Ca [117], Be [118], Fe [119], etc.) onto the Si(111)7×7 surface is known to result in the formation of a type of surface cluster, referred to as a ring-cluster (RC).

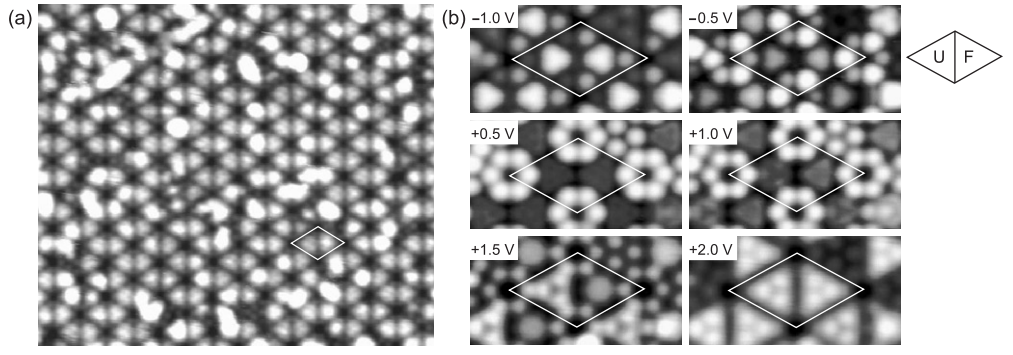

Figure 21. (a) Empty-state (+2.0 V) STM image (350×270 Å^2) of the Cu-SMC array prepared by deposition of ~0.4 ML Cu onto the Si(111)7×7 surface held at room temperature. (b) Bias-dependent STM appearance of the Cu/Si(111)7×7 magic clusters. STM images were acquired from the same clusters at various sample voltages, −1.0, −0.5, +0.5, +1.0, +1.5, and +2.0 V. The 7×7 unit cell is outlined. Schematic diagram on the right side of the figure illustrates location of the unfaulted (U) and faulted (F) halves within the 7×7 unit cell. [106].

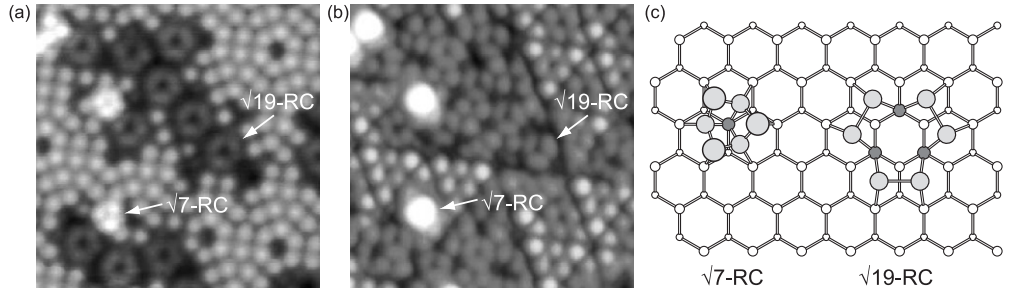

Figure 22. Random array of the ring clusters: (a) Empty-state (+2.0 V) and (b) filled-state (−0.8 V) STM images of the same 100×100 Å^2 region on the surface prepared by RT deposition of 0.5 ML of Fe onto Si(111)7×7 surface followed by annealing at 450°C. Ring clusters (RCs) of two types (indicated $\sqrt{7}$-RC and $\sqrt{19}$-RC constitute a random cluster array coexisted with a partially disrupted Si(111)7×7 surface. (c) Structural models of the $\sqrt{7}$-RC [114,115] and $\sqrt{19}$-RC [110].

They appear as three oval globe-shaped protrusions making a ring in the high-resolution STM images. Two well-defined types of RCs are observed in most of the above metal/Si(111) systems. Figure 22(a) and (b) show empty- and filled-state STM images of the same area of the Fe/Si(111) surface, in which the RCs of both types are present.

The RC of the first type (hereafter, $\sqrt{7}$-RC) shows up in the empty-state STM images as a group of three lobes centred in the on-top (T_1) site. They look brighter and smaller than the second type. In the filled-state STM images, the $\sqrt{7}$-RC shows up as a single bright protrusion. Close packing of these RCs produces a $\sqrt{7} \times \sqrt{7}R \pm 19.1^\circ$ lattice. From the metal coverage required to saturate the surface with the $\sqrt{7} \times \sqrt{7}$ structure (0.12–0.14 ML) [114], it has been established that each $\sqrt{7}$-RC contains only one metal atom. The structural model of the $\sqrt{7}$-RC, based on STM observations

[109,111,114,115] and quantitative ion scattering analysis [114], is shown in Figure 22(c). In the model, the metal atom replaces a Si atom in the top Si(111) surface layer and is surrounded by six Si adatoms above the surface to form a ring. Of these six adatoms, three (called 'bridge adatoms') are supposed to make bonds with the metal atom. They are located closer to the metal atom, and lower in height compared to the other three (called 'cap adatoms') [114,115]. Thus, the ring is threefold rather than sixfold symmetric.

The second type of RC (hereafter, $\sqrt{19}$-RC) shows up both in the empty- and filled-state STM images as a group of three lobes centred in the H_3 site. They are darker and larger. Close packing of these RCs produces a $\sqrt{19} \times \sqrt{19}R \pm 23.4^\circ$ lattice. In accordance with Auger electron spectroscopy data [108], $\sqrt{19}$-RC incorporates three metal atoms. In the tentative structural model based on STM observations [110] (see Figure 22c), each metal atom in the substitutional sites in the bottom of the Si(111) substrate bilayer is sixfold coordinated and each Si adatom in the six-member ring is 'bridge-bonded' with a metal atom and a surface Si atom in the top of the bilayer. In addition, Si adatoms in the ring are dimerised to reduce twice dangling bonds.

In most cases (especially, at low metal coverage), RCs are arranged randomly, forming the so-called '1×1'-RC phase [110–112,114,116], which displays a 1×1 LEED pattern due to the lack of long-range order of the clusters. Only two metals are known to induce the formation of ordered RC arrays. A-Si(111)$\sqrt{7} \times \sqrt{7}R \pm 19.1^\circ$-Co array was formed locally upon Co deposition followed by annealing at around 700°C [114,116]. The size of the $\sqrt{7} \times \sqrt{7}$-Co array is typically limited to < 50 Å [114]. A dual-polarity STM image of such a $\sqrt{7} \times \sqrt{7}$-Co array is shown in Figure 23(a) and (b). Similarly, nickel (0.2 ML) induced the formation of ordered RC array with $\sqrt{19} \times \sqrt{19}R \pm 23.4^\circ$ periodicity on the Si(111) at 550°C [113], as shown in Figure 23(c).

Very recently, interesting results were obtained by Ong and Tok [120], who used real-time STM observations to trace the process of self-assembly of the individual Co-SMCs on Si(111)7×7 into the $\sqrt{7} \times \sqrt{7}$ ordered array. Specifically, they found that hexagonal closed-packed structure consisting of seven SMCs is the smallest stable configuration. Borrowing the terminology from nucleation theory the critical nucleus size, i^*, is six clusters (rather than atoms).

4.4. *Pb-induced SMCs on Si(111)7 × 7*

The formation of the Pb-induced SMC lattice on the Si(111)7×7 surface was first reported in Ref. [121], in which the authors defined it as the 'borderline' magic clustering because the Pb-SMC growth takes place in a very narrow range of temperature (120 ± 20°C) and coverage. Furthermore, the transformation of the Pb-SMC into other forms of clusters by either losing or capturing Pb atoms is rather easy.

The STM image of a Pb-SMC ordered array obtained by depositing ~0.1 ML of Pb onto a Si(111)7×7 surface held at ~120°C is shown in Figure 24(a). The clusters occupy predominantly the faulted 7×7 HUCs, leaving the unfaulted HUCs nearly uncovered. The bias-dependent STM images of the Pb-SMCs are very different from other SMCs induced by Group-III or alkali metals, indicating that the Pb-SMC most likely has a different structure. Based on first-principles total-energy calculations, the model shown in Figure 24(b) has been chosen as the most energetically favourable. Its simulated STM images of both bias polarities agree well with the experimental results

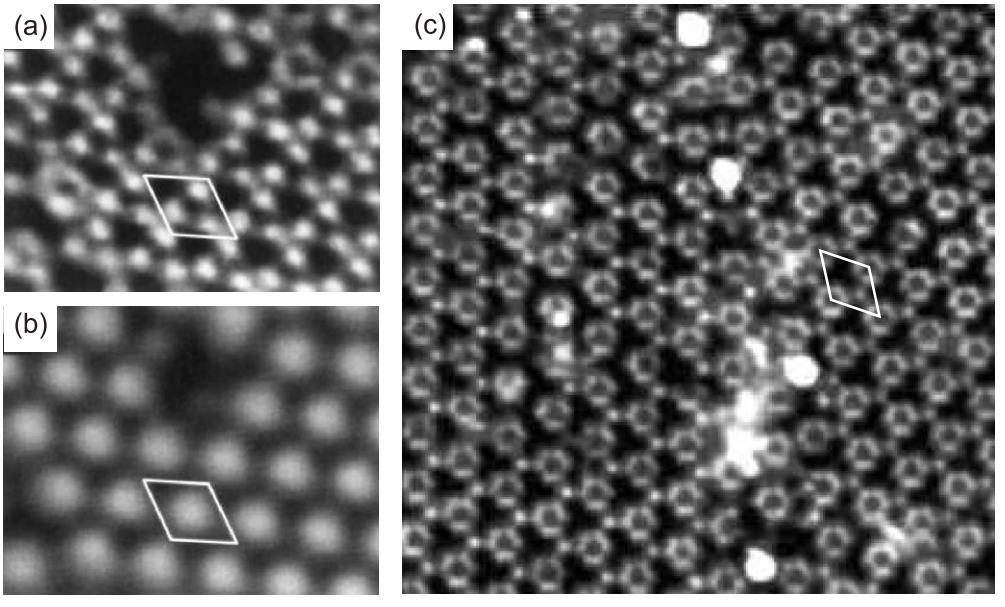

Figure 23. Ordered arrays of metal-induced ring clusters (RCs) on Si(111): (a) Empty-state (+2.0 V) and (b) filled-state (−1.8 V) STM images of the same 60×45 Å^2 region with the Si(111)$\sqrt{7} \times \sqrt{7}$-Co lattice domain [114]. (c) Filled-state (−2.3 V) 200×200 Å^2 STM image of the Si(111)$\sqrt{19} \times \sqrt{19}$-Ni array [113]. Unit cells of the arrays are outlined.

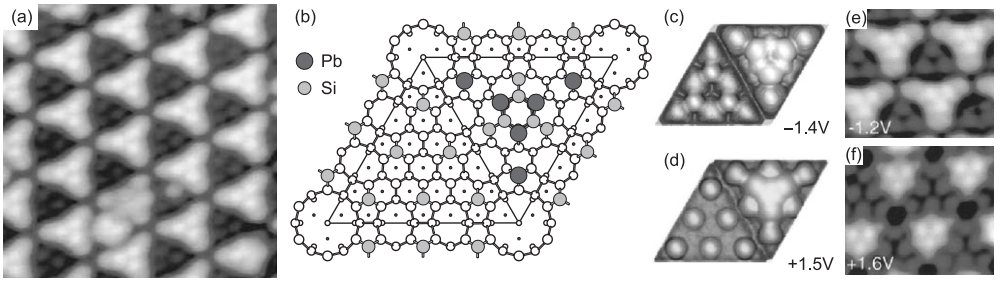

Figure 24. (a) Filled-state (−1.0 V) STM image (110×110 Å^2) of the Pb-induced SMC ordered array on Si(111)7×7. (b) Structural model of the Pb-SMC. Pb atoms are shown by the dark grey circles, edge Si-adatoms and 'ring Si-atoms' are shown by the light grey circles, other Si atoms are shown by the smaller white circles. Calculated (c) filled- and (d) empty-state STM images using the model in (b) with bias voltage −1.4 and +1.5 V, respectively. High-resolution STM images of the Pb-SMCs acquired at (e) −1.2 V and (f) +1.6 V [121].

(see Figure 24c–f). In the model, the three corner Si adatoms are replaced by Pb atoms and and join with three additional Pb atoms to form a ring in the centre of a HUC. Within the ring, each Si atom is bonded to the two neighbouring 'ring Pb-atoms' and an edge Si adatom; each Pb atom is bonded to the two neighbouring 'ring Si-atoms' and a Si rest-atom (Figure 24b). According to this model, the 'stoichiometry' of the SMC would be

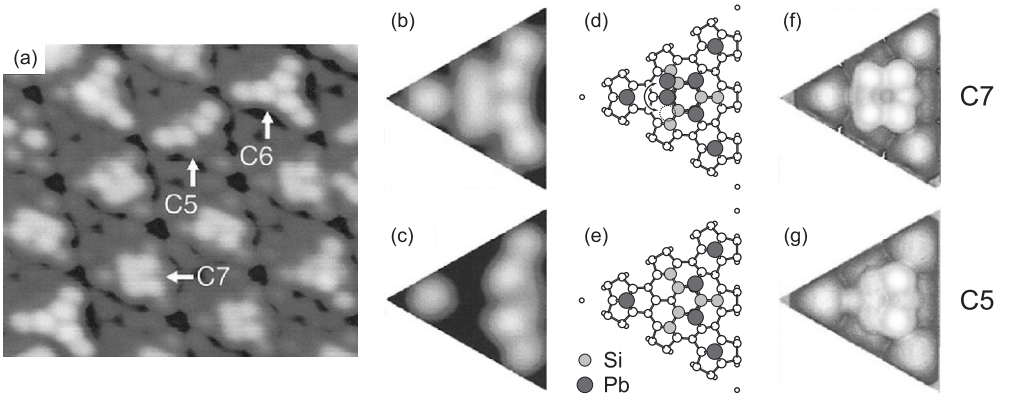

Figure 25. (a) Filled-state STM image ($90 \times 90\,\text{Å}^2$) of various Pb-induced clusters on Si(111)7×7. Labels C5, C6, and C7 indicate the three types of clusters. (b), (c) High-resolution experimental STM images, and (d), (e) calculated atomic structures for C7 and C5, respectively. The dashed-line circle in (d) represents the empty (mirror) bridge site, which is visited by the extra Pb atom in C7 and occupied in C8. (f), (g) Simulated STM images at $-1.4\,\text{V}$ [121].

described as Pb_3Si_6, for the three substituted Pb on the corners of a HUC do not have direct bonding to the SMC. Note that the exchange between Pb and corner Si has been suggested to be promoted by the exothermic formation of the clusters since this type of exchange has never been observed in the absence of the cluster phase at these growth temperatures.

A small deviation from the optimal growth conditions leads to the formation of more than two other kinds of clusters, as illustrated in Figure 25(a). Here, besides the 'normal' six-atom Pb-clusters (labelled C6 in Figure 25a), clusters with different STM images (labelled C5 and C7) were present. It has been concluded that C5 corresponds to the five-atom Pb cluster (i.e., one Pb atom missing from the normal cluster) and C7 to the seven-atom Pb cluster (i.e., one Pb atom added to the normal cluster). The proposed atomic structures for C5 and C7 are shown in Figure 25d and e. Their corresponding simulated STM images (Figure 25f and g) appear to be consistent with experimental results (Figure 25b and c). In the image simulation for C7, it has been assumed that the added Pb atom is mobile enough to be displaced back and forth (as illustrated by the arrow in Figure 25d) by the scanning tip to exhibit the bar-like feature on average. (The simulated image for C8 appears therefore to be indistinguishable from that of the averaged image for C7.) As a final remark, we would like to emphasize the conclusion drawn in Ref. [121], that the formation of various clusters is controlled largely by the growth kinetics rather than by surface thermodynamics.

4.5. *Tl-induced SMCs on Si(111)7 × 7*

The material system of Tl on Si(111)7×7 provides a special example in which ordered arrays of clusters with ill-defined complex structures or SMCs with different well-defined structures coexist on the surface, depending on the sample preparation procedure.

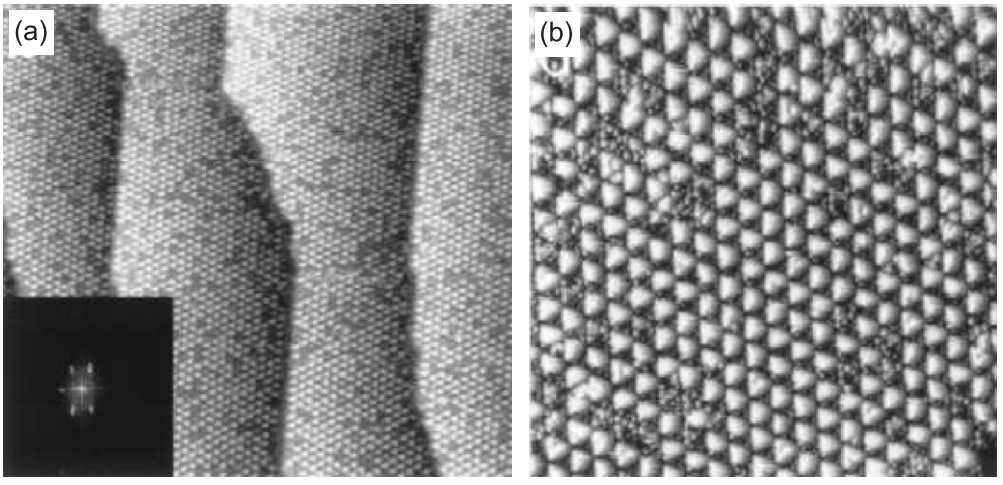

Figure 26. Filled-state (−2.0 V) STM images of an ordered array of Tl-clusters prepared by depositing ~0.2 ML of Tl onto a Si(111)7 × 7 surface at RT. (a) 1500 × 1500 Å^2; (b) 500 × 500 Å^2. The inset in (a) shows a Fourier transform of the image [122].

This system is quantitatively different from the Pb on Si(111)7 × 7 case, in which the coexisting clusters are of similar structure but different number of constituting atoms. The ordered arrays of Tl-clusters include an array of clusters with comparable size yet different complex structures formed on the 7 × 7 lattice at around RT; and arrays of three types of SMCs, each covering only a limited area, formed at higher temperatures. Such an interesting phenomenon of diverse magic clustering might be associated with the so-called 'inert pair effect' of the Tl atom's $6s^2$ electron configuration, which allows Tl to exhibit either one or three valences and therefore to bond with Si atoms in various configurations.

As demonstrated first by Vitali *et al*. [122,123], RT deposition of ~0.2 ML of Tl results in an ordered array of triangular Tl-clusters on the Si(111)7 × 7 surface. The clusters occupied almost exclusively the faulted HUCs, as shown in Figure 26. The clusters did not display a well-defined structure on the atomic scale and their sizes were not exactly identical. On average, each cluster was estimated to contain ~9 Tl atoms. With increasing Tl coverage beyond ~0.2 ML, the clusters added to the unfaulted HUCs merged with the existing clusters in the faulted HUCs and the Tl/Si(111) surface gradually lost its order [122,123]. Similar growth behaviour persisted for temperatures up to ~175°C, but from about 200°C (and up to ~350°C where Tl desorption becomes essential) another growth mode with diverse magic clustering can take place, as first reported by Zotov *et al*. [124]. With increasing Tl coverage (>0.2 ML), the Si(111)1 × 1-Tl phase [125–129] began to grow from the step edges and along the original 7 × 7 domain boundaries. Meanwhile on the surface regions where the 7 × 7 reconstruction was still preserved, ordered arrays of various Tl-SMCs were formed. At least three distinct types of the structurally well-defined Tl-SMCs have been detected [124] (Figure 27).

The most abundant Tl-SMC (hereafter, 1 × 1-SMC) comprised 15 Tl atoms occupying all of the T4 sites on the rest-atom layer of a 7 × 7 HUC (Figure 27a and b), whose atomic structure is equivalent to a small triangular domain of the Si(111)1 × 1-Tl reconstruction

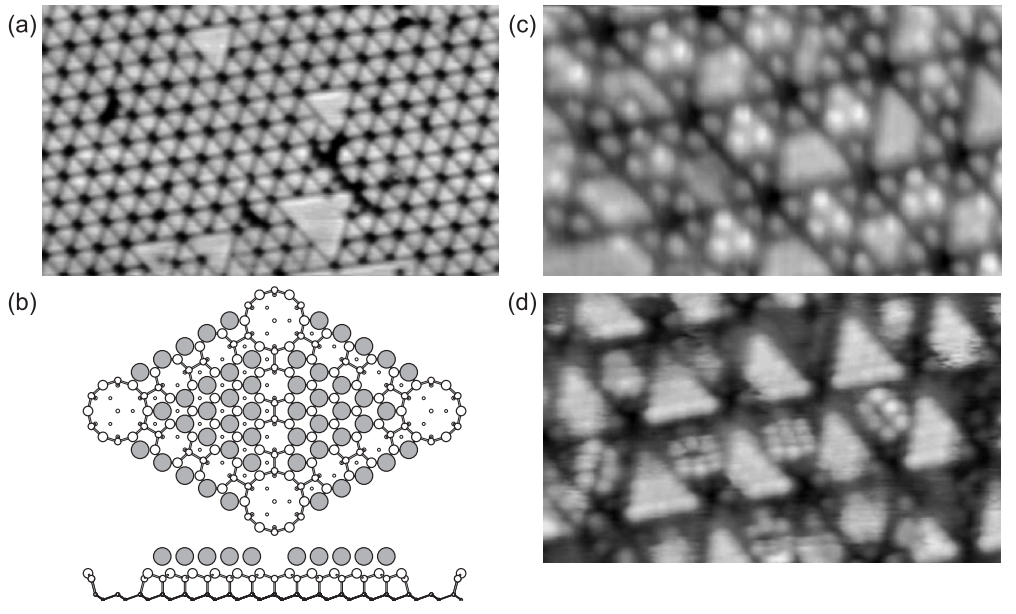

Figure 27. Ordered arrays of Tl-SMCs on the Si(111)7×7 surface. (a) Filled-state (-1.2 V) STM image (450×250 Å^2) and structural model of a Tl-SMC on a 7×7 unit cell. Each Tl-SMC is a triangular domain of the 1×1-Tl phase containing 15 Tl atom (shown by grey circles) on the T_4 sites within a 7×7 HUC. (c) Filled-state (-1.9 V) and (d) empty-state ($+1.8$ V) STM images (115×65 Å^2) of the arrays in which the faulted HUCs are occupied by the 1×1-SMCs and the unfaulted HUCs by the SMC of other two types [124].

induced by 1.0 ML Tl adsorption [125–129]. At a modest Tl coverage of below ~0.5 ML, the 1×1-SMC were located preferentially on the faulted HUCs, while the unfaulted HUCs were generally occupied by the clusters of the other two types, as shown in Figure 27(c) and (d). (Possible structures of these cluster types are discussed in Ref. [124]). When Tl coverage was increased to ~1.0 ML, almost all faulted and unfaulted HUCs become occupied by the 1×1-SMCs leading to the formation of the relatively large ordered arrays of the SMCs, as shown in Figure 27(a). Merging of the 15-atom SMCs took place occasionally and resulted in larger triangular 1×1 domains occupying $4, 9, 16, \ldots$ HUCs, as exemplified by the four 4-HUC and one 9-HUC domains in Figure 27(a). Such domains could be considered as clusters of a more stable 1×1-Tl phase grown at the expense of an ordered Tl-SMC array when the local Tl coverage approached closer and closer to 1.0 ML.

4.6. *Ag-SMCs on Pb/Si(111)*

The formation of Ag-SMCs on Pb/Si(111) [20] presents an interesting example in which the origin of the magic numbers of 2D metal clusters evolves from electronic to geometric shell closure as the SMC size increases, analogous to the case of 3D metallic magic clusters in free space. In Chiu's experiment [20], a stripe incommensurate phase was first prepared by depositing slightly more than 1 ML of Pb on a clean Si(111)7×7 surface at

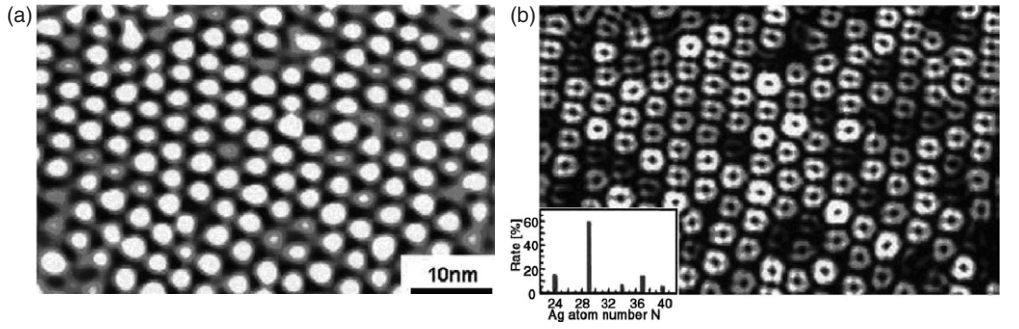

Figure 28. (a) An array of two-dimensional Ag nanoclusters with magic numbers of 24, 29, 34, 37, and 40 atoms. (b) Differentiating the corresponding topography image, the uniformity in size and shape of the nanoclusters is emphasized. Inset: histogram for size distribution [20].

RT followed by annealing the sample to 700 K. Then the sample was cooled to ~200 K and an extra amount of Pb was added to produce 2D Pb islands. On top of these islands, Ag clusters were fabricated using growth parameters described in Ref. [130]. Careful observations by STM revealed the existence of magic sizes in such nanoclusters. First-principles total-energy calculations suggested that the magic size originates from the electronic shell closing effect for the small cluster. For clusters beyond a certain size, the geometrical effect takes hold from the electronic effect as the major attribute. By exploiting the magic size effect of the Ag nanoclusters in conjunction with the preparation of Pb-islands with semi-periodical partitions, an ordered array of Ag-SMCs with a small number of size and shapes (Figure 28) was produced.

5. Properties of SMCs

So far, our understanding of the SMCs has been focused primarily on their formation process, chemical composition, and atomic structures. Very limited efforts have been devoted to studying their physical or chemical properties, which are among the most important issues concerning their intrinsic scientific interests and potential applications. In principle, one can apply several existing surface analytical techniques to examine their properties, but the lack of adequate spatial resolution or sensitivity of the techniques have led us to the present undesirable situation. To our knowledge, although the electronic properties of individual SMC has been examined using scanning tunnelling spectroscopy (STS), the physical properties of an ordered SMC-array has never been studied; and the first study on the catalytic property of an SMC-array was published only very recently [131].

In the following, we review cases where the properties of a SMC were studied by changing some its constituent atoms and the linkage between the structure/composition of the SMC with its properties was established. In retrospect, this seemingly natural way to explore the properties of a SMC by studying its response to cluster modification is not as easy as might be thought at first glance. By definition, a magic cluster has exclusively high stability just due to its specific closed-shell structure, hence it should in

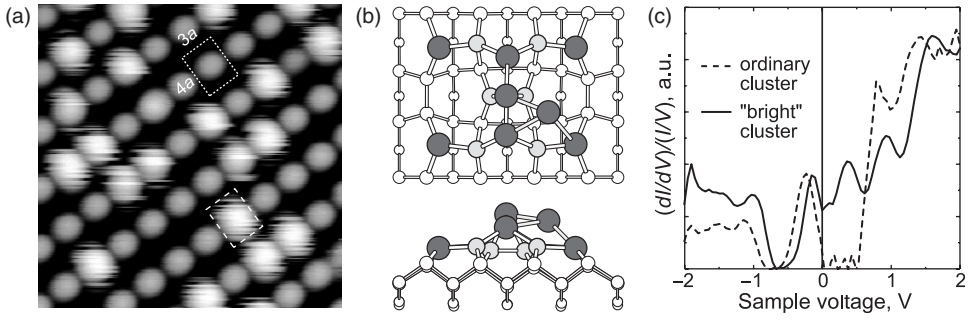

Figure 29. (a) Filled-state (−2.0 V) STM image ($100 \times 100\,\text{Å}^2$) of the In/Si(100)$4 \times 3$ SMC lattice with In-modified clusters. The ordinary cluster is outlined by a dotted frame, the modified cluster by a dashed frame. (b) Structural model of the modified In_8Si_6 cluster (top and side views). In atoms are shown by large dark-grey circles, Si atoms incorporated into the cluster by light-grey circles, Si atoms of the Si(100) substrate by small white circles. (c) $(dI/dV)/(I/V)$-versus-I STS spectra from the ordinary In_6Si_7 SMC (dashed line) and modified In_8Si_6 SMC (solid line) [133,136].

general resist attempts by foreign atoms to alter its energetically favourable atomic configuration. If the cluster modification nevertheless occurs, the modified cluster should also possesses highly-stable well-defined structure, in other words it is likely to be a magic cluster too. There were several attempts of SMC modification by depositing foreign atoms onto the pre-formed SMC arrays. Li *et al.* [59] deposited Ag onto the In-induced SMC lattice on Si(111)7×7 and reported formation of the In/Ag 'alloy' clusters, in which Ag atoms were suggested to reside atop the In_6Si_3 SMCs. Saito *et al.* [132] deposited Sb also onto the In-SMC 7×7 lattice and tentatively suggested the formation of $In_3Sb_3Si_3$ SMCs, i.e., In_6Si_3 SMCs in which the corner In atoms are replaced by Sb. More thorough investigations were devoted to elucidating the modification and the corresponding property change of the In_6Si_7 SMCs on Si(100) surface by the adsorption of In [133–136] and [Pb 137], therefore, we will discuss these cases in detail.

5.1. *Response of In/Si(100)4 × 3 SMCs to In adsorption*

When additional In was deposited onto the 4×3 lattice of In-SMCs on Si(100) at ~450°C (i.e., at the temperature of ~50°C lower than the optimum used for the In/Si(100)4×3 lattice formation), the array of modified SMCs exhibited a STM image as shown in Figure 29(a). The basic In/Si(100)4×3 SMC lattice was preserved, but some clusters appeared brighter and fuzzy. The fraction of the brighter clusters grows linearly with the In dose, and eventually reached the saturation of ~40% at ~0.05 ML of In. Quantitative evaluation of the modified-cluster composition yielded that each In_6Si_7 SMC cluster adopted two additional In atoms and lost 2 ± 1 Si atom. In the original publication [133], a symmetric In_8Si_5 model was proposed for the brighter cluster, which was ruled out in the subsequent more elaborate theoretical investigation [136], where the asymmetric In_8Si_6 model (Figure 29b) was found to have the lowest energy among the variety of possible candidates.

Results of STS demonstrated that the modification of the cluster (i.e., substitution of Si atoms within clusters by In atoms) altered its electronic properties (see Figure 29c). While the original In_6Si_7 SMCs STS spectrum exhibited a semiconductor behaviour with a band gap of ~0.6 eV, the modified cluster had an extra density of states within the band gap. The phenomenon is very similar to the doping of semiconductor crystals, and therefore the authors of Ref. [133] referred to it as SMC doping and coined the name of 'doped-SMC'.

One can see in Figure 29(b) that one of the additional In atoms is located in the cluster centre and the second In atom occupies the off-centred position. Calculations revealed that the most stable adsorption sites (S1) for the off-centred In-atom are those marked by squares in Figure 30(a). Note that there are four equivalent S1 sites within the cluster. To visit the neighbouring S1 site, i.e., that located in the same $2a \times 3a$ half of the 4×3 unit cell ($a = 3.84$ Å, the lattice constant of the Si(100)1×1 surface), an atom has to cross the saddle point S2 (marked by diamonds in Figure 30b). According to the calculations, this pathway has a barrier of 0.07 eV (Figure 30e). To visit the S1 site on the other $2a \times 3a$ half, two pathways are possible. The first is to go through the saddle point S3 (marked by triangles in Figure 30c) with a barrier of 0.71 eV (Figure 30e). The second pathway includes two steps: (i) In atom visits the S2 site; (ii) it replaces the central In atom by pushing it to the other $2a \times 3a$ half. This process proceeds through the formation of the configuration S4 shown in Figure 30(d) and is characterized by a barrier of 0.67 eV (Figure 30e). Thus, the calculated barriers for both pathways are very close. Such relatively low barriers suggest that all types of hopping pathways should be allowed at RT. In comparison, at 55 K, the hopping of an In atom between different $2a \times 3a$ halves should be frozen, but the hopping between S1 sites within the same half could still occur. Qualitatively, these results could explain the STM observations [136]. At RT, the cluster

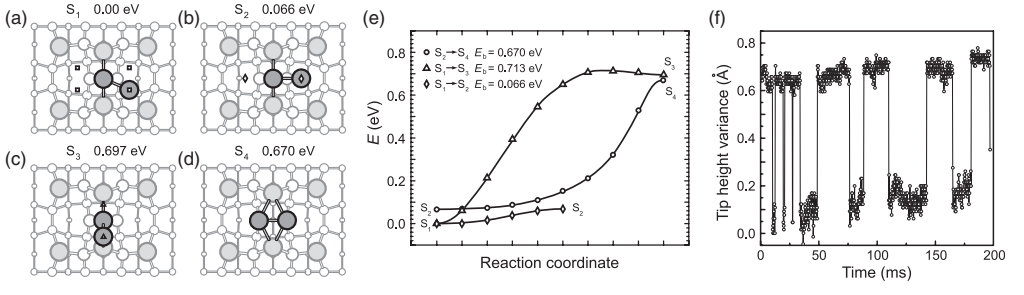

Figure 30. (a) Possible configurations occurring during hopping of the mobile In within a In_8Si_6 cluster, their formation energies and energetic barriers between them. (a) S1 configuration with mobile In atom in its ground state. There are four equivalent configurations of this type (marked by squares). (b) S2 configuration with In atom in a saddle point (marked by diamonds) while hopping to the nearest S1 site located in the same $2a \times 3a$ half of the cluster. (c) S3 configuration with In atom in a saddle point (marked by triangles) while hopping to the other $2a \times 3a$ half of the cluster. (d) S4 configuration occurring when mobile In atom substitutes the central In atom pushing it to the other half of the cluster. (e) Calculated shape of the barriers for different hopping pathways: diamonds for S1 → S2, triangles for S1 → S3 and circles for S1 → S4. The inset shows the values of the barrier height E_b (with respect to the S1-site level) for each pathway. (f) Tracking of the In-atom hopping between the $2a \times 3a$ halves by measuring the time dependence of the tip height in the off-centred point within the In_8Si_6 cluster [136].

appeared fuzzy due to hopping of In atom between neighbouring half unit cells. At 55 K, it appeared rigid and its centre was shifted along the 4*a* direction but not the 3*a* direction. (Since a STM image reflects the averaged view of the cluster, if the long-distance hopping along the 4*a* direction was frozen while short distance hopping along the 3*a* direction was still very fast, the centre of the cluster would appear shifted along the 4*a* direction.)

The dynamics of the RT hopping was directly detected by placing the STM tip off the centre of the cluster and monitoring the tip height (or tunnelling current) as a function of time (Figure 30f). When the mobile In atom was in the same half unit cell as the tip, the STM signal reached its high state; when it hoped to another half, the signal dropped to the low state, as shown in Figure 30(f). These interesting properties of the asymmetric In_8Si_6 cluster provided a conceptual starting point for the design of atomic switches, memory cells, or logic gates that can be used in future nanoelectronics.

5.2. *Response of In/Si(100)4 × 3 SMCs to Pb adsorption*

When Pb atoms were deposited onto the In/Si(100)4 × 3 SMC lattice at a temperature between 330 and 380°C, Pb-induced modification of the In-SMCs took place. The bias-dependent STM images of the Pb-modified clusters were different from that of the original In_6Si_7 SMC; in particular, their filled-state STM images appeared brighter, as illustrated in Figure 31(a). As shown by the structural model in Figure 31(b), the central Si atom of the original cluster is replaced by a Pb atom to form a symmetric In_6Si_6Pb structure. The model has the lowest energy according to first-principles total-energy calculations [137]. The simulated STM images of the model nicely reproduced all principal bias-dependent features of the experimental STM images, as demonstrated in Figure 32.

Remarkably, the modification of the Si(100)4 × 3-In SMC lattice by Pb could continue until an almost complete (up to 95%) array was achieved. In comparison, this is much better than the modification by In, where the fraction of In-modified clusters could never

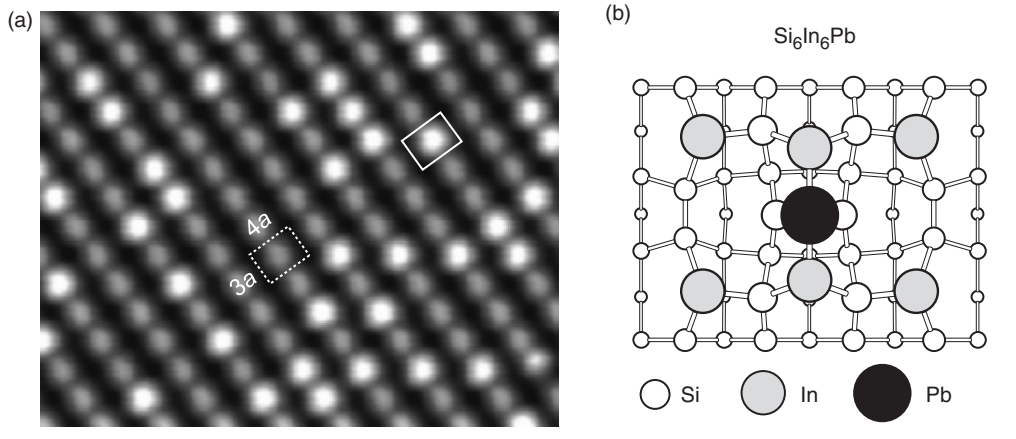

Figure 31. (a) Filled-state (−2.0 V) STM image (180 × 140 Å^2) of the In/Si(100)4 × 3 SMC lattice with the Pb-modified clusters. The ordinary cluster is outlined by a dotted frame, Pb-modified cluster by a solid frame. (b) Structural model of the Pb-modified In_6PbSi_6 cluster. The Pb atom is shown by the large dark-grey circle, In atoms by mediocre light-grey circles, Si atoms by small white circles [137].

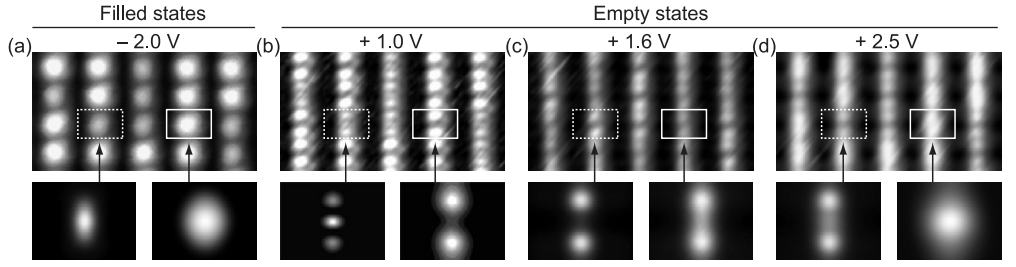

Figure 32. Comparison of the experimental (upper panel) and simulated (lower panel) STM images of the original In_6Si_7 cluster (outlined by a dotted frame in the experimental STM images) and Pb-modified In_6PbSi_6 cluster (outlined by a solid frame) at various bias voltages: (a) −2.0, (b) +1.0, (c) +1.6, (d) +2.5 V [137].

exceed ~40%. This difference could be understood since, according to total-energy calculations, the In-modified cluster, In_8Si_6, is less stable than the original In_6Si_7 cluster by ~30 meV [136], while the Pb-modified cluster, In_6PbSi_6, is, on the contrary, more stable by ~300 meV [137].

6. Discussion and conclusions

Recently, two cases of random SMC formation induced by the adsorption of small amounts of Co (~0.06 ML) [138,139] and Fe (~0.02 ML) [140] onto a Si(111)7 × 7 surface at ~150 to 250°C were reported. The SMCs occupied the off-centre positions in the 7 × 7 HUCs and broke their local threefold symmetry. Since the STM images of such a Co-SMC appeared almost identical to that of a Co-$\sqrt{7}$-RC described above (Figures 22 and 23), it is reasonable to speculate that both of them are of the same atomic structure. However, the authors of Refs. [138,140] suggested a cluster model consisting of six metal atoms and three edge Si adatoms displaced from their original sites, which is very different from the $\sqrt{7}$-RC model shown in Figure 22(c). More precise experimental measurement of the cluster's stoichiometry is needed to help clarify the issue. As a final remark on these systems, attempts to turn such random arrays of Co-SMCs or Fe-SMCs into ordered arrays by increasing the adsorbate coverage was not successful due to the formation of larger irregular clusters and the destruction of the 7 × 7 reconstruction locally.

There have been some reports of ordered arrays of adsorbate-induced clusters on the Si(111)7 × 7 surface exhibiting a rather sharp size distribution, which might be considered as an indication of the existence of SMCs. Although many of these adsorbates are chemically very different, they demonstrated very similar clustering behaviour. When adsorbed at temperatures close to RT, clusters of irregular shape and sizes were formed without destroying the 7 × 7 lattice reconstruction. Typically these clusters contained ~8–10 atoms on average and their size dispersion could reach ~10% in the best cases. This is better than most formation of clusters on surfaces, but obviously worse than that for SMCs. Although these clusters are not considered as SMCs for their lack of identical size and of well-defined structure under high resolution

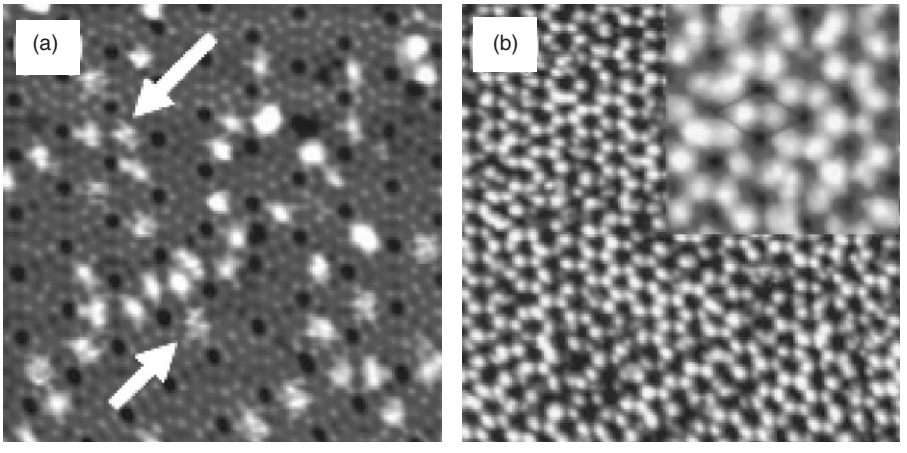

Figure 33. Formation of the Mn cluster array on Si(111)7 × 7 surface at room temperature. Empty-state (+2.0 V) STM images of the surface after depositing (a) ~0.04 and (d) ~0.56 ML of Mn. Scale: (a) $200 \times 200\,\text{Å}^2$, (b) $400 \times 400\,\text{Å}^2$. The arrows in (a) indicate the fuzzy features which plausibly corresponds to the Mn adatom migrating within the HUC. The inset in (b) shows the magnified STM image of the cluster array [141].

STM imaging, their general features are briefly discussed here for their relevance to the subject matter of this review.

Depending on the mobility of the adsorbate, the formation of such cluster arrays took place through two typical scenarios. For a low mobility adsorbate with little probability to move far away from its landing site, each cluster was usually confined within a HUC. At low coverages, irregular clusters were distributed randomly on the surface with a rather broad size distribution. As the coverage was increased, the growth of clusters exhibited a size self-limitation, which was controlled primarily by the potential landscape of the HUC. When the size reached the limit, it could not grow further because the arriving adatoms were likely to be repelled to the neighbouring partially filled HUCs. As a result of this self-limited growth, ordered arrays of clusters of similar sizes, occupying both the faulted and unfaulted HUCs, could be obtained on a Si(111)7 × 7 surface up to a certain coverage. This kind of cluster lattice manifests itself in the STM images as a quasi-crystalline honeycomb structure, as exemplified by depositing ~0.56 ML of Mn at RT [141] (Figure 33b). Very similar ordered cluster arrays had been reported for Sn [142], Pb [143], In [142], and Ge [144–147]. For an adsorbate with sufficient mobility to cross the boundaries of a HUC, its clustering behaviour was controlled largely by the thermodynamics. The migrating adatoms could 'feel' the energy difference between the faulted and unfaulted HUCs, hence the clusters were formed preferentially in the faulted HUCs. Agglomeration of adatoms into the cluster was governed by the progressively decreasing Gibbs free energy with increasing cluster size in conjunction with the size self-limitation imposed by the HUCs. The cluster size distribution was relatively sharp starting from low coverages. To illustrate this type of clustering we referred again to the adsorption of Mn, but this time at a higher temperature range of ~180–250°C [141,148]. As shown in Figure 34, the sizes of the Mn clusters remained almost constant with increasing

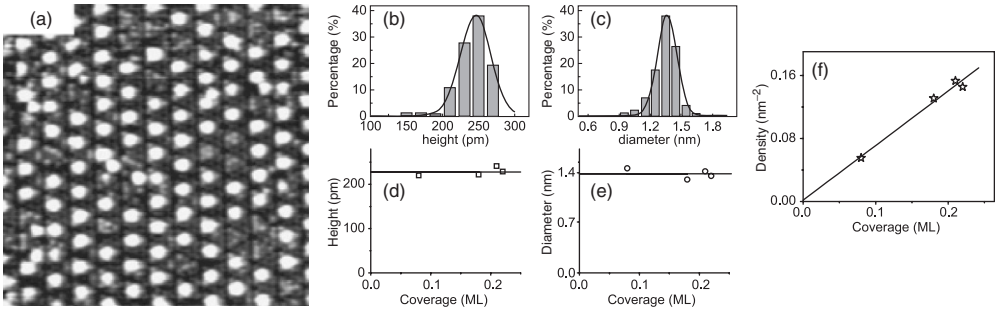

Figure 34. Formation of the Mn cluster array on a Si(111)7 × 7 surface at 180°C. (a) STM image (300×300 Å^2) of the cluster array at ~0.21 ML of Mn. (b) Height and (c) diameter distributions of the clusters shown in (a), (d), (e), and (f) are the height, diameter and areal density of the Mn clusters as a function of coverage [148].

Mn coverage, consequently the density of the Mn clusters increased linearly with the coverage up to ~0.21 ML of Mn, where the formation of a rather ordered cluster array was achieved. The Mn clusters occupied almost exclusively the faulted HUCs and each cluster contained ~11 Mn atoms on average. The dispersions in the cluster height and diameter were only 0.25 Å and 1.5 Å, respectively, which corresponds to 10% of the average height and diameter (hence, $\Delta S/S_a \sim 20\%$). The formation of similar cluster arrays had been reported for Tl [122,123], Ag [149,150], and Cr [151]. We would like to remark that the two growth modes suggested above provide only a very general idea of the interesting phenomenon of self-limited cluster growth. The real mechanism could be much more sophisticated and even mysterious. For example, quantitative analysis based on the rate equations and kinetic Monte Carlo simulations [152–155] have shown that random walk diffusion is insufficient to fit the aggregation rates and cluster size distribution, suggesting the occurrence of cooperative diffusion phenomena, whose physical nature still remains controversial.

The physical properties (electronic, magnetic, optical, mechanical, etc.) of SMCs and ordered SMC-arrays have been barely studied. The number of papers addressing these subjects is extremely limited. Only work-function measurements of Na-SMC [94,95] and Tl-SMC [156] lattices on a Si(111)7 × 7 surface, angle-resolved photoemission spectroscopy study of Na-SMC on Si(111)7 × 7 [95], and first-principles DFT calculations of the electronic properties of In-SMC and Al-SMC lattices on Si(111)7 × 7 [157] have been conducted. Much more effort along these lines is certainly needed to assess the prospects of the SMCs and SMC-arrays for technological applications such as semiconductor nanodevices.

Chemical properties of SMCs and SMC-arrays are of both fundamental importance and technological interests. For example, it is conceivable that a SMC-array might possess novel catalytic properties in certain surface reactions. Unfortunately, our knowledge in this aspect is as limited as that of the physical properties. Only very recently, an interesting result in this area has been reported [131]. Dissociation of methanol on various 2D Al overlayers on a Si(111) surface, including the Al-SMC lattice, the Al/Si(111)γ-phase, and the bulk-like 16-ML thick Al film was studied.

The surface with the Al-SMC lattice had the highest activity for the dissociation of CH_3OH while the bulk Al film showed the lowest activity. Furthermore, the CH_3OH reaction pathway varied with the surface structure. On the bulk Al film, the CH_3OH decomposition proceeded through O–H bond scission followed by C–O bond scission, which is the same as that on a bulk Al surface. On the surface of a Al-SMC lattice, the O–H bond scission and the C–O bond scission appeared to take place in parallel to produce surface OH species. Such a mechanism is only found to be active in the CH_3OH reactions on transition-metal surfaces [131]. Apparently, further studies about the surface chemistry of SMCs are necessary before we can fully understand the mysterious nature of such a concerted bond scission process and appreciate the breadth and depth of the chemistry of SMCs.

Potential applications of a SMC lattices can be used as a template surface for the overgrowth of various types of nanostructures. For example, in Refs. [158,159], self-organized Co nanoplatelets with a singular height, quantized lateral sizes, and unique shape and orientation have been reported to grow on the Al-SMC lattice on a Si(111)7×7 surface. The Co-nanoplatelet arrays exhibited interesting magnetic properties, namely, these nanomagnets had unusually high blocking temperatures (>100 K), despite their small volume of only a few nm^3. Pan *et al.* [159] speculated that the perpendicular easy axis for magnetization and the easy tunability of the lateral size of the nanomagnets made them highly desirable for potential applications in magnetic recording. Another potential application of a SMC-lattice was studied in the formation of In-islands on the surface of a pristine and modified In/Si(100)4×3 SMC lattices [160]. It was demonstrated that the shape and area density of the 2D In-islands could be controlled by first 'doping' an In-SMC lattice with In at higher temperature and then depositing the In at RT to form the islands. It is conceivable that SMC lattices will be exploited as templates for the growth of nanostructure arrays with novel properties.

The discovery of random SMCs on Ga/Si(111) system triggered some theoretical efforts to study the stability of 2D clusters with similar structures in free space [36], specifically, the stability of $Ga_{n(n+1)/2}Si_{n(n-1)/2}H_{3n+n(n-1)/2}$ clusters ($n = 2$, 3, and 4), whose structures are essentially the same as the Ga–Si bilayer model for the SMC except the cluster-surface connections were replaced by Ga–H and Si–H bonds. The results of the calculation include several features that help us understand the properties of this type of cluster. First both $Ga_{n(n+1)/2}Si_{n(n-1)/2}H_{3n+n(n-1)/2}$ and $Ga_{(n+1)/2}Si_{n(n-1)/2}(SiH_3)_{3n}H_{n(n-1)/2}$ clusters ($n = 2, 3$, and 4) are triangular and thermodynamically stable. The Si–Ga bond strength in the clusters is calculated to be 1.74–1.83 eV. Such a large bond energy helped explain why the presence of dangling Si bonds in the vicinity of a SMCs on the $\sqrt{3} \times \sqrt{3}R30^\circ$ reconstructed Ga/Si(111) surface could affect its stability. It would be very interesting if such 2D triangular clusters could be synthesized and characterized.

Although the energies of Ga-, In-, and Al-SMCs have been calculated using first-principles calculations, the degrees of their shell closure remain unknown. In order to gain deeper understanding of SMCs, it is necessary to be able to calculate energies of clusters on a particular surface as a function of their sizes. In principle, this can be done, but it is very demanding because there are usually numerous possible atomic structures of the clusters as well as the surface. Clearly, more effective theoretical tools are needed

before we can have precise quantitative understanding of the energetics of SMC. The required computing power is even more demanding, if our goal is to be able to predict the existence of certain SMCs. In the foreseeable future, it appears that experimentalists and theorists have to work together to try to understand why and how certain SMCs exist.

The existence of the class of III_6Si_3 SMC lattices on the Si(111) surface should not be treated as an exception rather than common rule. The reduction in the number of dangling bonds in a unit cell and the complete bonding satisfaction of the cluster itself are good energetic arguments for 'predicting' the enhanced stability of the Ga-, In-, and Al-SMCs. However, they are certainly not a sufficient condition for expecting that deposition of any group III elements Si(111)7×7 surface would lead to the formation of 2D SMC lattices. The known exception of the 'rule of thumb for SMC formation' is that, at room temperature, Tl deposition on Si(111)7×7 leads to formation of an ordered array of nanodots with liquid-like structures rather than SMCs with identical structures. It is clear that subtle differences in the bonding energy and strain energy of the adsorbed layer as well as the growth kinetics of the adsorbates could lead to a result that does not always coincide with the intuitive expectation. Another counter-intuitive example can be found in the long-period 8×8-reconstructed Si_3N_4 (0001) surface, which seems to be an appropriate template to achieve an ordered clustering. However, deposition of Co [161] resulted in neither spatial cluster ordering nor SMC formation.

The research on SMCs and ordered arrays of SMCs is still in its early stage of development. Only a few cases of SMC lattices have been unambiguously confirmed by both experiment and theory. We have reviewed the highlights of the recent developments in this interesting new frontier with some emphasis on their implications to the fabrication of a precisely ordered array of identical nanostructures. So far, the studies have been concentrated on the creation and structure determination of SMCs as well as lattices of SMCs. The potential applications of SMCs and ordered SMC-arrays in the emerging nanoscience and nanotechnology are very appealing. For example, the ability to form an array of identical magnetic nanocluster may find important applications in the area of surface nanomagnetism [162]. The catalytic property of SMCs could be further explored for conversion of gases by taking advantage of their particular quantum size effects, similar to the case of Au nanoclusters [163]. Since all of the known SMC lattices were found on the Si surface, it appears natural to consider the integration of such an ordered array of identical nanostructures with the existing Si technology. There is no intrinsic limitation in exploiting SMC lattices as bases for building massive arrays of ultrahigh density electric nanodevices. However, many technical obstacles need to be overcome before such integration can take place. For example, the sizes of SMCs discovered so far are too small to be integrated with the existing Si technology. In principle, the size limitation could be overcome by using a template with a larger surface lattice unit cell, but the search for such a template is an interesting and challenging subject in itself. An alternative is to develop brand new connection technologies that would allow contacts to these small SMCs. But again, the development is likely to take a long time. In summary, the scientific interests and potential applications of SMCs and SMC-arrays are extremely attractive and exciting. With our limited understanding of these fascinating nanostructures, much more

research is needed before we can start to take advantage of their quantum properties and precise translational symmetry.

Acknowledgements

We would like to thank Prof. C. M. Wei for his valuable suggestions. This work was partly supported by the National Science Council of Taiwan (NSC96-2120-M-001-002) and Russian Foundation for Basic Research (05-02-90571-HHC and 07-02-00650-a).

References

[1] D. M. Tennant, in *Nanotechnology*, edited by G. Timp (Springer-Verlag, New York, 1999).
[2] D. M. Eigler and E. K. Schweizer, Nature **344**, 524 (1990).
[3] E. J. Heller, M. F. Crommie, C. P. Lutz, *et al*., Nature **369**, 464 (1994).
[4] E. T. Foley, A. F. Kam, J. W. Lyding, *et al*., Phys. Rev. Lett. **80**, 1336 (1998).
[5] F. Moresco, G. Meyer, K.-H. Rieder, *et al*., Phys. Rev. Lett. **86**, 672 (2001).
[6] S.-W. Hla, L. Bartels, G. Meyer, *et al*., Phys. Rev. Lett. **85**, 2777 (2000).
[7] A. P. Alivisatos, Science **271**, 933 (1996).
[8] J. L. Wilbur and G. M. Whitesides, in *Nanotechnology*, edited by G. Timp (Springer-Verlag, New York, 1999).
[9] G. Springholz, V. Holy, M. Pinczolits, *et al*., Science **282**, 734 (1998).
[10] C. T. Black, C. B. Murray, and R. L. Sandstrom, Science **290**, 1131 (2000).
[11] H. Brune, M. Giovannini, K. Bromann, *et al*., Nature **394**, 451 (1998).
[12] J. Tersoff, C. Teichert, and M. G. Lagally, Phys. Rev. Lett. **76**, 1675 (1996).
[13] V. A. Shchukin and D. Bimberg, Rev. Mod. Phys. **71**, 1125 (1999).
[14] L. Brus, in *Nanotechnology*, edited by G. Timp (Springer-Verlag, New York, 1999), pp. 257–284.
[15] W. D. Knight, K. Clemenger, Walt A. de Heer, *et al*., Phys. Rev. Lett. **52**, 2141 (1984).
[16] M. Brack, Scientific American. **277**, 50 (1997).
[17] H. Häkkinen and M. Manninen, Phys. Rev. Lett. **76**, 1599 (1996).
[18] M. Manninen, Physics World **11**, 24 (1998).
[19] Y. L. Wang and M. Y. Lai, J. Phys.: Cond. Matt. **13**, R589 (2001).
[20] Y. P. Chiu, L. W. Huang, C. M. Wei, *et al*., Phys. Rev. Lett. **97**, 165504 (2006).
[21] G. Rosenfeld, A. F. Becker, B. Poelsema, *et al*., Phys. Rev. Lett. **69**, 917 (1992).
[22] T. Michely, M. Hohage, S. Esch, *et al*., Surf. Sci. **349**, L89 (1996).
[23] M. Y. Lai and Y. L. Wang, Phys. Rev. Lett. **81**, 164 (1998).
[24] M. Y. Lai and Y. L. Wang, Phys. Rev. B **60**, 1764 (1999).
[25] B. Voigtländer, M. Kästner, and P. Šmilauer, Phys. Rev. Lett. **81**, 858 (1998).
[26] I. S. Hwang, M. S. Ho, and T. T. Tsong, Phys. Rev. Lett. **83**, 120 (1999).
[27] M. Otsuka and T. Ichikawa, Jpn. J. Appl. Phys. **24**, 1103 (1985).
[28] M. Zinke-Allmang and L. C. Feldman, Surf. Sci. **191**, L749 (1987).
[29] T. Thundat, S. M. Mohapatra, B. N. Dev, *et al*., J. Vac. Sci. Technol. A. **6**, 681 (1988).
[30] J. Zegenhagen, M. S. Hybertsen, P. E. Freeland, *et al*., Phys. Rev. B **38**, 7885 (1988).
[31] D. M. Chen, J. A. Golovchenko, P. J. Bedrossian, *et al*., Phys. Rev. Lett. **61**, 2867 (1988).
[32] J. R. Patel, J. Zegenhagen, P. E. Freeland, *et al*., J. Vac. Sci. Technol. B. **7**, 894 (1989).
[33] J. Zegenhagen, J. R. Patel, P. Freeland, *et al*., Phys. Rev. B **39**, 1298 (1989).
[34] J. Zegenhagen, P. F. Lyman, M. Böhringer, *et al*., Phys. Status Solidi(b) **204**, 587 (1997).
[35] M. Y. Lai and Y. L. Wang, Phys. Rev. B **61**, 12608 (2000).
[36] A. M. Mebel, M. Y. Lai, and Y. L. Wang, Chem. Phys. Lett. **318**, 27 (2000).
[37] S. F. Tsay, M. H. Tsai, M. Y. Lai, *et al*., Phys. Rev. B **61**, 2699 (2000).

[38] K. Takayanagi, Y. Tanishiro, S. Takahashi, *et al.*, Surf. Sci. **164**, 367 (1985).
[39] K. Cho and E. Kaxiras, Europhys. Lett. **39**, 287 (1997).
[40] M. Y. Lai and Y. L. Wang, Phys. Rev. B **64**, 241404 (2001).
[41] J. F. Jia, X. Liu, J. Z. Wang, *et al.*, Phys. Rev. B **66**, 165412 (2002).
[42] J. F. Jia, J. Z. Wang, X. Liu, *et al.*, Nanotechnology **13**, 736 (2002).
[43] S. Gangopadhyay, T. Schmidt, and J. Falta, Surf. Sci. **552**, 63 (2004).
[44] H. H. Chang, M. Y. Lai, J. H. Wei, *et al.*, Phys. Rev. Lett. **92**, 066103 (2004).
[45] M. A. Van Hove, W. H. Weinberg, and C. M. Chan, *Low Energy Electron Diffraction* (Springer, Heidelberg, 1986), Vol. Vol. 6, Springer Series in Surface Science.
[46] A. Ohtake, Phys. Rev. B **73**, 033301 (2006).
[47] J. Jia, J. Z. Wang, X. Liu, Q. K. Xue, *et al.*, Appl. Phys. Lett. **80**, 3186 (2002).
[48] V. G. Kotlyar, A. V. Zotov, A. A. Saranin, *et al.*, Phys. Rev. B **66**, 165401 (2002).
[49] M. Yoshimura, K. Takaoka, T. Yao, *et al.*, Phys. Rev. B **47**, 13930 (1993).
[50] M. Yoshimura, K. Takaoka, T. Yao, *et al.*, J. Vac. Sci. Technol. B **12**, 2434 (1994).
[51] K. Nishikata, K. Murakami, M. Yoshimura, *et al.*, Surf. Sci. **269/270**, 995 (1992).
[52] E. A. Khramtsova, A. V. Zotov, A. A. Saranin, *et al.*, Appl. Surf. Sci. **82/83**, 576 (1994).
[53] H. Narita, M. Kakeya, A. Kimura, *et al.*, e-J. Surf. Sci. Nanotech. **4**, 208 (2006).
[54] H. Narita, A. Kimura, M. Taniguchi, *et al.*, Phys. Rev. B **76**, 115405 (2007).
[55] R. W. Li, H. Liu, J. H. G. Owen, *et al.*, Phys. Rev. B **76**, 075418 (2007).
[56] R. W. Li, S. Kusano, J. H. G. Owen, *et al.*, Nanotechnology **17**, 2018 (2006).
[57] R. W. Li, J. H. G. Owen, S. Kusano, *et al.*, Appl. Phys. Lett. **89**, 073116 (2006).
[58] M. Saito, H. Sasaki, M. Mori, *et al.*, e-J. Surf. Sci. Nanotech. **3**, 244 (2005).
[59] J. L. Li, J. F. Jia, X. J. Liang, *et al.*, Phys. Rev. Lett. **88**, 066101 (2002).
[60] J. C. Li and Q. Jiang, Appl. Surf. Sci. **226**, 327 (2004).
[61] X. F. Lin, H. A. Mai, I. Chizhov, *et al.*, J. Vac. Sci. Technol. B **14**, 995 (1996).
[62] M. Yoon and R. F. Willis, Surf. Sci. **512**, 255 (2002).
[63] J. Kraft, M. G. Ramsey, and F. P. Netzer, Phys. Rev. B **55**, 5384 (1997).
[64] V. G. Kotlyar, unpublished.
[65] S. H. Ke, T. Uda, and K. Terakura, Phys. Rev. B **62**, 15319 (2000).
[66] S. Y. Tong, H. Huang, C. M. Wei, *et al.*, J. Vac. Sci. Technol. A **6**, 615 (1988).
[67] T. Uchihashi, Y. Sugawara, T. Tsukamoto, *et al.*, Phys. Rev. B **56**, 9834 (1997).
[68] R. L. Lo, M. S. Ho, I. S. Hwang, *et al.*, Phys. Rev. B **58**, 9867 (1998).
[69] C. M. Chang and C. M. Wei, Phys. Rev. B **67**, 033309 (2003).
[70] H. W. Yeom, T. Abukawa, M. Nakamura, *et al.*, Surf. Sci **341**, 328 (1995).
[71] A. A. Baski, J. Nogami, and C. F. Quate, Phys. Rev. B **43**, 9316 (1991).
[72] A. A. Saranin, A. V. Zotov, V. G. Lifshits, *et al.*, Phys. Rev. B **60**, 14372 (1999).
[73] O. Bunk, G. Falkenberg, L. Seehofer, *et al.*, Appl. Surf. Sci. **123/124**, 104 (1998).
[74] O. Bunk, G. Falkenberg, J. H. Zeysing, *et al.*, Phys. Rev. B **60**, 13905 (1999).
[75] M. Shimomura, T. Nakamura, K. S. Kim, *et al.*, Surf. Rev. Lett. **6**, 1097 (1999).
[76] E. P. J. Reese, T. Miller, and T. C. Chiang, Phys. Rev. B **64**, 233307 (2001).
[77] T. M. Schmidt, P. J. L. Castineira, and R. H. Miwa, Surf. Sci. **482/485**, 1468 (2001).
[78] N. Takeuchi, Phys. Rev. B **63**, 245325 (2001).
[79] J. Cotzomi-Paleta, G. H. Cocoletzi, and N. Takeuchi, Surf. Rev. Lett. **9**, 1641 (2002).
[80] T. M. Schmidt, P. J. L. Castineira, and R. H. Miwa, Appl. Phys. Lett. **79**, 203 (2001).
[81] G. H. Cocoletzi and N. Takeuchi, Surf. Sci. **504**, 101 (2002).
[82] V. G. Zavodinsky, Surf. Sci. **516**, 203 (2002).
[83] J. H. Seo, J. Y. Park, S. K. Jung, *et al.*, Chem. Phys. Lett. **417**, 72 (2006).
[84] V. G. Kotlyar, A. A. Saranin, A. V. Zotov, *et al.*, Surf. Sci. **506**, 80 (2002).
[85] V. G. Kotlyar, A. V. Zotov, A. A. Saranin, *et al.*, e-J. Surf. Sci. Nanotech. **1**, 33 (2003).
[86] M. Kishida, A. A. Saranin, A. V. Zotov, *et al.*, Appl. Surf. Sci. **237**, 110 (2004).
[87] A. A. Saranin, A. V. Zotov, V. G. Kotlyar, *et al.*, Phys. Rev. B **71**, 035312 (2005).

[88] H. Sakama, A. Kawazu, T. Sueyoshi, *et al*., Phys. Rev. B **54**, 8756 (1996).
[89] Y. Nakada and H. Okumura, J. Vac. Sci. Technol. B **16**, 645 (1998).
[90] Y. Nakada, I. Aksenov, and H. Okumura, J. Vac. Sci. Technol. B **17**, 1 (1999).
[91] N. Shimizu, H. Kitada, and O. Ueda, Phys. Rev. B **51**, 5550 (1995).
[92] N. Shimizu, H. Kitada, and O. Ueda, J. Cryst. Growth **150**, 1159 (1995).
[93] Y. Oshima, T. Hirata, T. Yokoyama, *et al*., Surf. Sci. **465**, 81 (2000).
[94] K. Wu, Y. Fujikawa, T. Nagao, *et al*., Phys. Rev. Lett. **91**, 126101 (2003).
[95] J. R. Ahn, K. Yoo, J. T. Seo, *et al*., Phys. Rev. B **72**, 113309 (2005).
[96] K. Wu, Y. Fujikawa, T. Briere, *et al*., Ultramicroscopy **105**, 32 (2005).
[97] K. Wu, Y. Fujikawa, Y. Takamura, *et al*., Chin. J. Phys. **43**, 197 (2005).
[98] K. H. Wu, A. I. Oreshkin, Y. Takamura, *et al*., Phys. Rev. B **70**, 195417 (2004).
[99] K. Cho and E. Kaxiras, Surf. Sci. **396**, L261 (1998).
[100] C. Zhang, G. Chen, K. Wang, *et al*., Phys. Rev. Lett. **94**, 176104 (2005).
[101] K. Wu, Sci. Technol. Adv. Mater. **6**, 789 (2005).
[102] A. Watanabe, M. Naitoh, and S. Nishigaki, Jpn. J. Appl. Phys. **37**, 3778 (1998).
[103] St. Tosch and H. Neddermeyer, Surf. Sci. **211/212**, 133 (1989).
[104] T. Yasue, T. Koshikawa, H. Tanaka, *et al*., Surf. Sci. **287/288**, 1025 (1993).
[105] Y. P. Zhang, L. Yang, Y. H. Lai, *et al*., Surf. Sci. **531**, L378 (2003).
[106] A. V. Zotov, D. V. Gruznev, O. A. Utas, *et al*., Surf. Sci. **602**, 391 (2008).
[107] R. J. Wilson and S. Chiang, Phys. Rev. Lett. **58**, 2575 (1987).
[108] T. Ichinokawa, T. Tani, and A. Sayama, Surf. Sci. **219**, 395 (1989).
[109] S. A. Parikh, M. Y. Lee, and P. A. Bennett, J. Vac. Sci. Technol. A **13**, 1589 (1995).
[110] S. A. Parikh, M. Y. Lee, and P. A. Bennett, Surf. Sci. **356**, 53 (1996).
[111] T. Yao, S. Shinabe, and M. Yoshimura, Appl. Surf. Sci. **104/105**, 213 (1996).
[112] G. Kinoda and K. Ogawa, Surf. Sci. **461**, 67 (2000).
[113] J. Gutek, S. Szuba, and R. Czajka, Acta Physica Polonica A **104**, 345 (2003).
[114] P. A. Bennett, M. Copel, D. Cahill, *et al*., Phys. Rev. Lett. **69**, 1224 (1992).
[115] M. H. Tsai, J. D. Dow, P. A. Bennett, *et al*., Phys. Rev. B **48**, 2486 (1993).
[116] R. J. Phaneuf, P. A. Bennet, M. Marsi, *et al*., Surf. Sci. **431**, 232 (1999).
[117] A. A. Saranin, V. G. Lifshits, K. V. Ignatovich, *et al*., Surf. Sci. **448**, 87 (2000).
[118] D. A. Hite, S. J. Tang, and P. T. Sprunger, Chem. Phys. Lett. **367**, 129 (2003).
[119] M. V. Ivanchenko, E. A. Borisenko, V. G. Kotlyar, *et al*., Surf. Sci. **600**, 2623 (2006).
[120] W. J. Ong and E. S. Tok, Phys. Chem. Chem. Phys. **9**, 991 (2007).
[121] S. C. Li, J. F. Jia, R. F. Dou, *et al*., Phys. Rev. Lett. **93**, 116103 (2004).
[122] L. Vitali, M. G. Ramsey, and F. P. Netzer, Phys. Rev. Lett. **83**, 316 (1999).
[123] L. Vitali, F. P. Leisenberger, M. G. Ramsey, *et al*., J. Vac. Sci. Technol. A **17**, 1676 (1999).
[124] A. V. Zotov, A. A. Saranin, V. G. Kotlyar, *et al*., Surf. Sci. **600**, 1936 (2006).
[125] S. S. Lee, H. J. Song, N. D. Kim, *et al*., Phys. Rev. B **66**, 233312 (2002).
[126] T. Noda, S. Mizuno, J. Chung, *et al*., Jpn. J. Appl. Phys. **42**, L319 (2003).
[127] V. G. Kotlyar, A. A. Saranin, A. V. Zotov, *et al*., Surf. Sci. **543**, L663 (2003).
[128] N. D. Kim, C. G. Hwang, J. W. Chung, *et al*., Phys. Rev. B **69**, 195311 (2004).
[129] K. Sakamoto, P. E. J. Eriksson, S. Mizuno, *et al*., Phys. Rev. B **74**, 075335 (2006).
[130] H. Y. Lin, Y. P. Chiu, L. W. Huang, *et al*., Phys. Rev. Lett. **94**, 136101 (2005).
[131] Z. Zhang, Q. Fu, H. Zhang, *et al*., J. Phys. Chem. **111**, 13524 (2007).
[132] M. Saito, C. Takeuchi, M. Mori, *et al*., Appl. Surf. Sci. **244**, 137 (2005).
[133] V. G. Kotlyar, A. V. Zotov, A. A. Saranin, *et al*., System Phys. Rev. Lett. **91**, 026104 (2003).
[134] J. R. Ahn, J. H. Byun, W. H. Choi, *et al*., Phys. Rev. B **70**, 113304 (2004).
[135] H. Jeong and S. Jeong, J. Korean. Phys. Soc. **48**, 98 (2006).
[136] A. A. Saranin, A. V. Zotov, I. A. Kuyanov, *et al*., Phys. Rev. B **74**, 125304 (2006).
[137] A. V. Zotov, O. A. Utas, V. G. Kotlyar, *et al*., Phys. Rev. B **76**, 115310 (2007).
[138] M. A. K. Zilani, Y. Y. Sun, H. Xu, *et al*., Phys. Rev. B **72**, 193402 (2005).

[139] M. A. K. Zilani, H. Xu, T. Liu, *et al*., Phys. Rev. B **73**, 195415 (2006).
[140] M. A. K. Zilani, Y. Y. Sun, H. Xu, *et al*., Surf. Sci. **601**, 2486 (2007).
[141] H. Wang and Z. Q. Zou, Appl. Phys. Lett. **88**, 103115 (2006).
[142] M. Yoon, X. F. M. Lin, I. Chizhov, *et al*., Phys. Rev. B **64**, 085321 (2001).
[143] D. Tang, H. E. Elsayed-Ali, J. Wendelken, *et al*., Phys. Rev. B **52**, 1481 (1995).
[144] Y. P. Zhang, L. Yan, S. S. Xie, *et al*., Surf. Sci. **497**, L60 (2002).
[145] L. Yan, Y. Zhang, H. Gao, *et al*., Surf. Sci. **506**, L255 (2002).
[146] Z. A. Ansari, T. Arai, and M. Tomitori, Surf. Sci. **574**, L17 (2005).
[147] H. F. Ma, Z. H. Qin, M. C. Xu, *et al*., Phys. Rev. B **75**, 165403 (2007).
[148] D. Y. Wang, L. J. Chen, W. He, *et al*., J. Phys. D **39**, 347 (2006).
[149] J. Mysliveček, P. Sobotík, I. Oštádal, *et al*., Phys. Rev. B **63**, 045403 (2001).
[150] P. Kocán, P. Sobotík, I. Oštádal, *et al*., Surf. Sci. **566/568**, 216 (2004).
[151] O. A. Utas, T. V. Utas, V. G. Kotlyar, *et al*., Surf. Sci. **596**, 53 (2005).
[152] C. Polop, E. Vasco, J. A. Martín-Gago, *et al*., Phys. Rev. B **66**, 085324 (2002).
[153] E. Vasco, C. Polop, and E. Rodríguez-Cañas, Phys. Rev. B **67**, 235412 (2003).
[154] E. Vasco, Phys. Rev. B **69**, 075412 (2004).
[155] E. Vasco, Surf. Sci. **575**, 247 (2005).
[156] C. G. Hwang, N. D. Kim, G. Lee, *et al*., Appl. Phys. A **89**, 431 (2007).
[157] L. Zhang, S. B. Zhang, Q. K. Xue, *et al*., Phys. Rev. B **72**, 033315 (2005).
[158] T. Xie, A. Kimura, S. Qiao, *et al*., J. Phys.: Cond. Matt. **16**, S5783 (2004).
[159] M. H. Pan, H. Liu, J. Z. Wang, *et al*., Nano Lett. **5**, 87 (2005).
[160] A. A. Saranin, A. V. Zotov, V. G. Kotlyar, *et al*., Surf. Sci. **598**, 136 (2005).
[161] X. Liu, J. F. Jia, J. Z. Wang, *et al*., Chin. Phys. Lett. **20**, 1871 (2003).
[162] P. Gambardella, S. Rusponi, M. Veronese, *et al*., Science **300**, 1130 (2003).
[163] M. Valden, X. Lai, and D. W. Goodman, Science **281**, 1647 (1998).